THE UNIVERSITY OF MANITOBA

Avalanche Breakdown and Microplasma Noise in Space-Charge-Limited Anthracene Diode

by

Donald K.M. Yau

A Thesis

Submitted to the Faculty of Graduate Studies

in Partial Fulfillment of the Requirements for the Degree

of Master of Science

DEPARTMENT OF ELECTRICAL ENGINEERING

Winnipeg, Manitoba

October, 1972

ABSTRACT

The current-voltage (I-V) characteristics of a space-charge-limited anthracene diode near the breakdown region has been studied. A physical model for microplasma noise in the space-charge-limited solid-state diode has been developed. The temperature dependence of breakdown voltage has been measured. The results show that the postbreakdown current decreases as the temperature is increased and the breakdown voltage increases with increase of temperature. The onset of microplasma breakdown is used to measure the temperature coefficient of the breakdown voltage. This measurement has been justified by comparing the results obtained from silicon p-n junctions and the existing data published in the literature. The temperature dependence of the threshold voltage is in reasonable agreement with the theory.

Low frequency noise measurement is performed on the device. Low frequency excess noise is found to be caused by the bulk effect. The results show that the low frequency noise has a f^{-1} dependence.

The effect of pulsed radiation on the I-V characteristic has also been investigated. We found that although the steady-state photoresistivity of an anthracene space-limited diode is very large, it is a poor light detection device for pulsed type of irradiation.

TABLE OF CONTENTS

LIST OF FIGURES

(LIST OF FIGURES - continued)

ACKNOWLEDGEMENTS

The author would like to express his thanks to Dr. S.T. Hsu for his invaluable advice and continuous encouragement. He is also indebted to all the technical staff of Electrical Engineering of the University of Manitoba for their laboratory assistance.

CHAPTER I

INTRODUCTION

Anthracene $C_{14}H_{10}$ has served as a model system for attempts to understand molecular crystals. The avalanche breakdown phenomena in inorganic semiconductors have been studied very extensively in the past twenty years. This breakdown can be either radiative or nonradiative. Avalanche breakdown with associated light emission on a single-hole-injection space-charge-limited anthracene diode has been observed by Hsu [22] . Large amplitude noise arising from current instability at the onset of breakdown was noted by the author and was found to be microplasma noise. McKay [33] showed that in silicon, during the microplasma instability, practically all the current is carried by a series of current pulses of constant amplitude but of random lengths and occurrence. At the very onset of breakdown these pulses are very short so that total current is small; as the voltage is increased above that at which pulses first appear, the pulses are observed to increase slightly in amplitude, to have much longer average duration and to be of more frequent occurrence, until a voltage is reached at which the current remains flowing continuously. At higher voltages other similar sets of pulses may occur. These observations by McKay suggested localized breakdown regions (microplasmas), each of which requires a slightly different breakdown sustaining voltage

and each having a range of voltages in which the localized breakdown is bistable. This interpretation was confirmed by Chynoweth and Pearson [7] who observed recombination radiation from individual microplasmas in shallow diffused junctions; they were able to correlate the onset of each set of light spot in the junction with the onset of each set of current pulses observed.

Ideal p-n junction diodes exhibit V-I characteristics with a sharply defined breakdown point under reverse bias. In general, practical solid state devices do not have a sharply defined breakdown point. There is always an uncertainty in the breakdown voltage that is due to soft junction, and so there is always a bend or a knee around the breakdown point indicating the transition region. In this thesis, the author attempts to take care of the breakdown voltage by noting the onset of microplasmas. Experimental work was carried out by using the above assumption to determine the temperature coefficient which was then compared with the established data. The end result has indicated a favourable justification of this assumption. Low frequency noise and photo effects on anthracene are also investigated.

Chapter II presents a brief review of the previous theoretical analysis on the avalanche breakdown mechanism in semiconductor devices and some of the experimental results obtained by several investigators. In Chapter III, an analysis of microplasma phenomenon is presented and a model of 'turn-on'

and 'turn-off' of microplasma in anthracene is proposed. The experimental techniques are given in Chapter IV. Chapter V presents experimental data. The analysis of the experimental data is discussed in Chapter VI. Finally, conclusions are drawn from the experimental observations as presented in Chapter VII.

CHAPTER II

AVALANCHE BREAKDOWN IN SEMICONDUCTORS

2.1 REVIEW ON AVALANCHE BREAKDOWN AND BASIC CONCEPTS

In order to have a thorough understanding and to fully utilize the characteristics of avalanche breakdown diodes, it is necessary to gain some understanding of the basic theories that govern the breakdown mechanism. Physically, junction breakdown in excess of eight volts is the process of secondary ionization or avalanche breakdown. The basic mechanism of avalanche breakdown is similar to the Townsend discharge in gas-filled tubes. It relies on the ionization of carriers and on impact collision of atoms by other carriers which have been imparted sufficient energy by an electric field. Suppose a free electron or hole exists within the depletion layer of the junction and an electric field is applied. An increased velocity in the direction of the electric field and hence an increase in the carrier's kinetic energy, is given to the free carrier. As a result of the lattice structure in the crystal, the free carrier may collide with an atom within the junction and, because of its high energy level, may knock off carriers from the atom. If sufficient energy still remains in the original colliding carrier, additional collisions will occur and thus other carriers will be freed from additional atoms. The newly released carriers now gain sufficient energy from the field to initiate

new collisions. Although some breakdown in solid crystals relying only on the ionization of electrons have been observed [58], generally it is necessary that both electrons and holes be ionized in order to provide the positive feedback or regenerative mechanism [33].

McKay [33] , [34] has shown that even before the junction breaks down completely, a given carrier injected into the depletion layer of the reverse-biased junction results in a current flow greater than that of injected carrier. Thus a multiplication of carrier has occurred. When the applied voltage across the junction approaches the breakdown voltage, V_B, the multiplication factor increases very rapidly and, in fact, the point of breakdown is defined as the point at which the multiplication factor, M, becomes infinite.

In addition to the actual breakdown, the multiplication effect produces additional results, such as, any degree of reverse leakage currents will be multiplied in the region of prebreakdown, thus producing a certain amount of softness in the characteristic curve, especially at elevated temperatures.

McKay [33] expressed the value of M mathematically as;

$$M = \frac{1}{1 - \int_0^W \alpha_i \, dx} \qquad \ldots(1)$$

where α_i is the rate of ionization and w is the effective width of the actual junction.

Miller [35] has given a relation evolved from observation for the multiplication factor in step junctions:

$$M = \frac{1}{1 - (V_R/V_B)^n} \qquad \ldots(2)$$

where V_R is the applied voltage, V_B is the body breakdown voltage due to avalanche, and n is the number that depends on the resistivity and the resistivity type of the high-resistivity side of the junction.

The rate of ionization α_i is defined as the number of hole-electron pairs produced by a given carrier per cm. of path travelled in the direction of the field. The ionization rate is slightly different for holes and electrons and is also a function of the semiconductor material and the applied field. In equation (1), McKay assumed that the ionization rates for holes and electrons were equal.

The value of α_i and its dependence on the strength of the applied electric field were investigated by Chynoweth [8], who found from experiment that the ionization rate obeyed a function in the empirical form of

$$\alpha_i(E) = a\, e^{-(b/E(r)^m)} \qquad \ldots(3)$$

where E is the value of the electric field and a, b, and m are empirical constants. Maserjian [29] has shown that for an abrupt junction the values of the constant a for silicon and germanium are 9×10^5 and 1.2×10^7, respectively. The values of b for silicon and germanium are 1.8×10^6 and 1.4×10^6

respectively.

Mathematically we may define the point of breakdown as being the condition

$$\int_o^W \alpha_i \, dx = 1 \qquad \ldots(4)$$

One significant parameter in any theory of breakdown is the temperature coefficient. McKay [33] observed that the multiplication curve of a junction has the same temperature coefficient as the breakdown voltage. The temperature dependence of the avalanche breakdown voltage for linear-gradient junctions can be described approximately by

$$V_B(T) = V_B(T_o)[1 + \beta'(T - T_o)] \qquad \ldots(5)$$

where $V_B(T_o)$ = breakdown voltage at room temperature T_o

$V_B(T)$ = breakdown voltage at the temperature T

β' = temperature coefficient.

McKay [33] established that all junctions showed positive temperature coefficients for the multiplication characteristics. The coefficient was defined by $(1/V_a)(dV_a/dT)$ for a given value of the multiplication. The extent of the variation of the junction width with temperature is usually negligible. From (5), the field dependence on temperature was deduced to be

$$E_B(T) = E_B(T_o)[1 + \beta\,(T-T_o)] \qquad \ldots(6)$$

where $E_B(T)$ = maximum field at breakdown at temperature T

$E_B(T_o)$ = breakdown field at temperature T_o

$$\beta = 0.5\ \beta' \ .$$

To derive from this the temperature coefficient of α_i (7), we let $M \to \infty$. McKay showed that

$$\frac{1}{\alpha_i}\left[\frac{\partial \alpha_i}{\partial T}\right] = -\beta \left\{1 + \frac{E_B}{\alpha_i}\left[\frac{\partial \alpha_i}{\partial E_B}\right]_T\right\} \qquad \ldots(7)$$

where all quantities are evaluated at $T = T_o$. $\frac{\partial \alpha_i}{\partial E_B}$ can be obtained by differentiating the curve plotted as ionization rate α_i verses electric field E, so that if β is known, $\frac{\partial \alpha_i}{\partial T}$ can be determined or vice-versa. It should be noted that equation (7) is applicable only to step junctions and is subject to the assumption of equation (1).

In general, the definition of breakdown voltage V_B is the value of reverse voltage that causes the diode to enter the breakdown or high reverse current region. If all the diodes has a characteristic in which the transition from reverse leakage to breakdown was as sharply defined as an ideal diode, it would be easy to define V_B as the voltage at the exact point of transition. Unfortunately, this is not the case in general. In many cases the breakdown transition has a certain softness in the knee region. The end result is that a meaningful specification of the breakdown voltage V_B must include a specification of the reverse current I_R at which it is to be measured. The temperature at which the test is performed and the thermal resistance between the device leads and the ambient can also influence the value of V_B. There is always an uncertainty in the breakdown voltage V_B due to

soft junction.

Avalanche breakdown was observed in homogeneous materials as well as in p-n junction. Anthracene is a molecular semiconductor and exhibits avalanche breakdown under high voltage. The sample used was a conventional single injection space-charge-limited diode. The fact that the postbreakdown current decreased as the temperature was increased was justified that breakdown was an avalanche. The breakdown voltage varied as temperature was varied. If the current-voltage curve was used to specify the breakdown value, the expected breakdown point would be such that the current increased very rapidly with voltage. However, in space-charge-limited diodes, this breakdown voltage is not well-defined; thus the conventional I-V curve would not give a clear picture at breakdown.

2.2 THEORETICAL CALCULATION OF AVALANCHE BREAKDOWN

The mathematical calculation of breakdown mechanism in ordinary p-n junctions is analyzed as follows:

Let α_n = electron ionization rate, i.e. the number of electron-hole pairs generated by one electron travelled a unit distance;

α_p = hole ionization coefficient.

In general, the ionization rates for electrons and holes are different. Therefore α_n is not equal to α_p. It is assumed that the depletion width of a junction under study is as that

shown in Figure 1.1, where I_{po} is the incident current at left-hand side of the depletion region. Through the process of secondary ionization the hole current will increase with distance through the junction and reach a value MI_{po} at the right-hand side of the junction. Since at steady state the total current is constant,

$$I = I_p + I_n \qquad \ldots(1)$$

There are I_n/q electrons per second and I_p/q holes per second crossing the differential section dx. The hole current $I_p(x)$ changes by an amount equal to the number of electron-holespairs generated per second in the range dx (times electronic charge) or the increment of hole current is

$$dI_p = \alpha_p I_p dx + \alpha_n I_n dx$$

i.e.
$$\frac{dI_p}{dx} = \alpha_n I + (\alpha_p - \alpha_n) I_p \qquad \ldots(2)$$

Equation (2) has a solution subject to a boundary condition.

$$I = I_p(W) = M_p I_{po} \qquad \ldots(3)$$

It is assumed that at x = W the electron current is negligibly small compared to the hole current. Similarly,

$$I = M_n I_{no} = I_n(o) \qquad \ldots(4)$$

This approximation can be made only when M_n, $M_p >> 1$.

$$I_p(x) = I\left\{\frac{1}{M_p} + \int_o^x \alpha_n \exp\left[-\int_o^x (\alpha_p-\alpha_n)\, dx'dx\right]\right\}$$
$$\cdot \exp\left[\int_o^x (\alpha_p-\alpha_n)\, dx\right] \qquad \ldots(5)$$

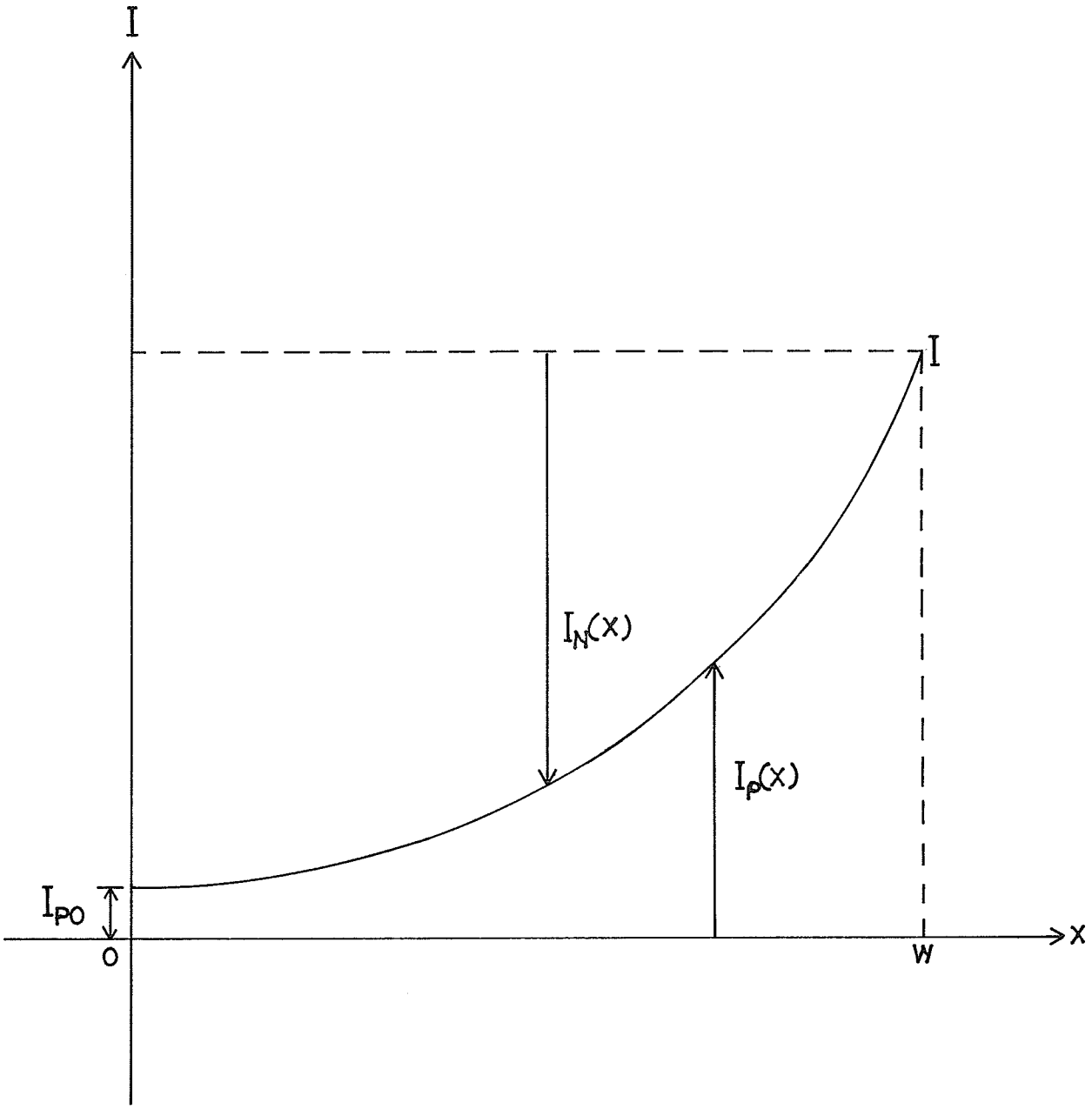

FIG. 2.1. CURRENT DISTRIBUTION IN DEPLETION REGION.

where M_p is the multiplication factor for holes and is defined as

$$M_p = \frac{I_p(W)}{I_p(o)} = \frac{I}{I_p(o)} \qquad \ldots(6)$$

since $I_p(W)$ and the total current I are identical. The multiplication factor is obtained from (5) and (6). From (5) we can write

$$I_p(x) = \frac{I\{\frac{1}{M_p} + \int_o^x \alpha_n \exp\left[-\int_o^x (\alpha_p-\alpha_n)\, dx'\right]dx\}}{\{\exp\left[-\int_o^x (\alpha_p-\alpha_n)\, dx'\right]\}}$$

$$I_p(x)\ \{\exp\left[-\int_o^x (\alpha_p-\alpha_n)\, dx'\right]\} = I\{\frac{1}{M_p} + \int_o^x \alpha_n \exp\left[-\int_o^x (\alpha_p-\alpha_n)dx'\right]dx\}$$

as $I_p(W) = I$, at $x = W$, we have

$$\exp\{-\int_o^W (\alpha_p-\alpha_n)\, dx'\] = \frac{1}{M_p} + \int_o^W \alpha_n \exp\{-\int_o^x (\alpha_p-\alpha_n)\, dx'\}dx$$

$$\therefore\ \frac{1}{M_p} = \exp\left[-\int_o^W (\alpha_p-\alpha_n)\, dx\right] - \int_o^W \alpha_n \exp\{-\int_o^X (\alpha_p-\alpha_n)\, dx'\}dx$$

$$\ldots(7)$$

Now

$$\int_o^W (\alpha_n-\alpha_p) \exp\left[-\int_o^x (\alpha_p-\alpha_n)\, dx'\right]dx$$

$$= \exp\left[-\int_o^x (\alpha_p-\alpha_n)\, dx'\right]\Big|_{x=o}^{W}$$

$$= \exp\left[-\int_o^W (\alpha_p-\alpha_n)\, dx\right] - 1 \qquad \ldots(8)$$

From (7) and (8) we have

$$\frac{1}{M_p} = \exp\left[-\int_o^W (\alpha_p-\alpha_n)\, dx\right] - \int_o^W (\alpha_n-\alpha_p) \exp\left[-\int_o^x (\alpha_p-\alpha_n)dx'\right]dx$$

$$- \int_o^W \alpha_p \exp\left[-\int_o^x (\alpha_p-\alpha_n)\, dx'\right]dx$$

$$\frac{1}{M_p} = \exp\left[-\int_o^W (\alpha_p-\alpha_n)dx\right] - \exp\left[-\int_o^W (\alpha_p-\alpha_n)dx\right] + 1 - \int_o^W (\alpha_p-\alpha_n)dx'\Big]dx$$

$$\therefore\ 1 - \frac{1}{M_p} = \int_o^W \alpha_p \exp\left[-\int_o^x (\alpha_p-\alpha_n)\, dx'\right]dx \qquad \ldots(9)$$

The breakdown voltage V_B is defined as the voltage where M becomes infinite. If the ionization rates for electrons and holes are the same, breakdown occurs where an electron (or hole) produces exactly one secondary on the average in one transit. If the ionization rates are different, then the carrier which ionizes most must produce more than one secondary to compensate for the other type of carrier which causes lesser ionization. It can be shown that the breakdown condition is symmetrical. That is, if

$$\int_o^W \alpha_p \exp\left[-\int_o^x (\alpha_p-\alpha_n)\, dx'\right]dx = 1\ ,$$

then

$$\int_o^W \alpha_n \exp\left[-\int_x^W (\alpha_n-\alpha_p)\, dx'\right]dx = 1\ . \qquad \ldots(10)$$

Experimentally it is found that

$$\alpha_n \text{ or } \alpha_p = \alpha_o \left(\frac{E}{E_o}\right)^n \qquad \ldots(11)$$

where α_o and E_o are constants and $\alpha = \alpha_\infty \exp\,(-b/E)^m$

where b is an electric field that is in general different

from $\xi_i/q\ell$, if ξ_i is the ionization threshold and ℓ is the mean free path, respectively.

To extend the multiplication integral over a wide range of multiplication it is necessary to account for ionization by both electrons and holes.

Let

$$\alpha_p = \gamma\ \alpha_n \qquad \ldots(12)$$

With the assumption of constant γ, the multiplication integral (9) becomes

$$1 - \frac{1}{M_p} = \frac{\gamma}{1-\gamma}\left\{\exp\left[-\left(1-\frac{1}{\gamma}\right)\int_o^W \alpha_p\ dx\right] - 1\right\}$$

$$1 - \frac{1}{M_n} = \frac{1}{\gamma-1}\left\{\exp\left[\int_o^W (\gamma-1)\ \alpha_n\ dx\right] - 1\right\} \qquad \ldots(13)$$

where the value of γ should be chosen at the maximum field. Avalanche breakdown occurs at

$$\int_o^W \alpha_n\ dx = \frac{\ell_n \gamma}{\gamma-1}$$

or

$$\int_o^W \alpha_p\ dx = \frac{\gamma \ell_n \gamma}{\gamma-1} \qquad \ldots(14)$$

2.2.1 Step Junction

A step junction is defined as having constant impurity density on either side of an abrupt step on density, as in Figure 1.2(a). The field varies linearly with distance, and the width W is related to voltage V by

$$V = \frac{NqW^2}{2\varepsilon} \qquad \ldots(15)$$

where

$$\frac{1}{N} = \frac{1}{N_D} + \frac{1}{N_A}$$

ε = permittivity

V = sum of applied and 'built-in' voltage.

The maximum field is

$$E_m = 2\,\frac{V}{W} = \frac{qNW}{E}$$

and

$$E(x) = 2\,\frac{V}{N} \cdot \frac{x}{W} \qquad \ldots(16)$$

where E is assumed to be zero at x = 0. Actually, equation (16) strictly applies only to one-sided junctions (i.e. $N_D >> N_A$). For junctions that have significant width on both sides of the junction, E(x) must be represented by two straight lines. Figure 2.2 shows a one-sided equivalent for a two-sided step junction.

The ionization integral is

$$\int_o^W \alpha dx = \int_o^W \alpha_\infty \, e^{-bw^2/2Vx} \, dx \qquad \ldots(17)$$

Let z = x/w, then

$$\int_o^W \alpha dx = \alpha_{max} \, W_{eff} \qquad \ldots(18)$$

$$W_{eff} = W \int_o^1 \exp\left[\left(1 - \frac{1}{z}\right) \frac{b}{E_{max}}\right] dz \qquad \ldots(19)$$

The determination of the ionization integral involves (i) determination of E_{max} and (ii) determination of α_{max} and

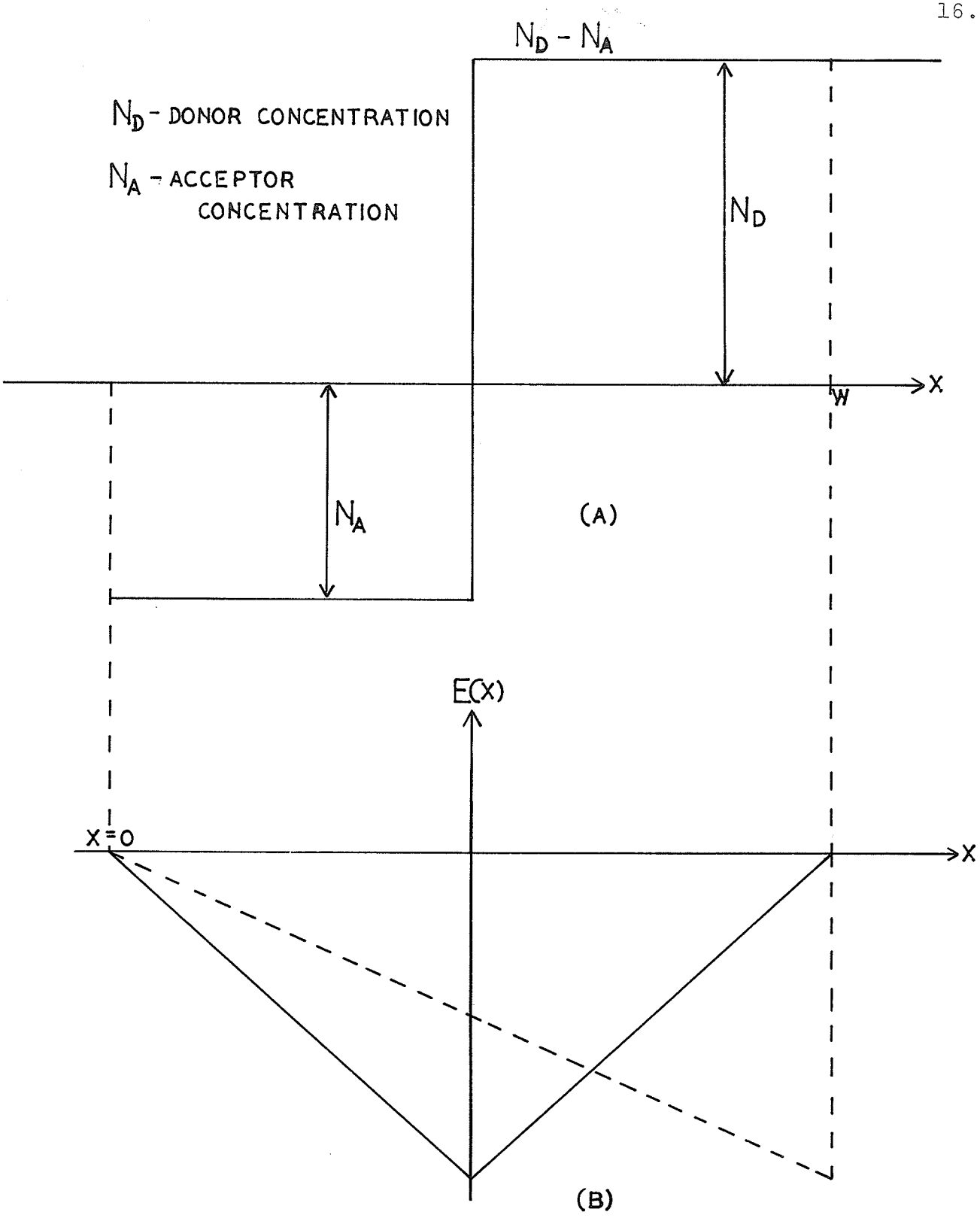

FIG. 2.2(A). IMPURITY DENSITY IN A STEP JUNCTION.

(B). FIELD DISTRIBUTION IN A STEP JUNCTION.

W_{eff}. Assuming that $m = \frac{b}{E_o} >> 1$, the empirical forms are as follows,

$$1 - \frac{1}{M_n} \simeq \frac{\ell_n \gamma}{\gamma - 1} \left(\frac{V}{V_B}\right)^{(m+1)/2}$$

$$1 - \frac{1}{M_p} \simeq \frac{\gamma \ell_n \gamma}{\gamma - 1} \left(\frac{V}{V_B}\right)^{(m+1)/2} \qquad \ldots(20)$$

2.2.2 Linearly Graded Junctions

A linearly graded junction is defined as having a constant slope in net impurity density as shown in Figure 2.3. In a linearly graded junction,

$$\rho = q\, ax \;, \; -x_o < x < x_o \qquad \ldots(21)$$

$$E = \frac{-qa}{E} \; \frac{x_o^2 - x^2}{2} \qquad \ldots(22)$$

$$V = \frac{qa\, W^3}{12E} \qquad \ldots(23)$$

where V = voltage across junction

a = gradient of impurities

$W = 2x_o$ = junction width

The ionization integral is

$$1 - \frac{1}{M_n} = \int_o^W \alpha_n \, dx$$

$$= 2 \int_o^{W/2} \alpha_\infty \exp \left\{ - \frac{b}{\frac{qa}{2E}\left[\left(\frac{W}{2}\right)^2 - x^2\right]} \right\} dx$$

$$= \alpha_{max} \, W_{eff} \qquad \ldots(24)$$

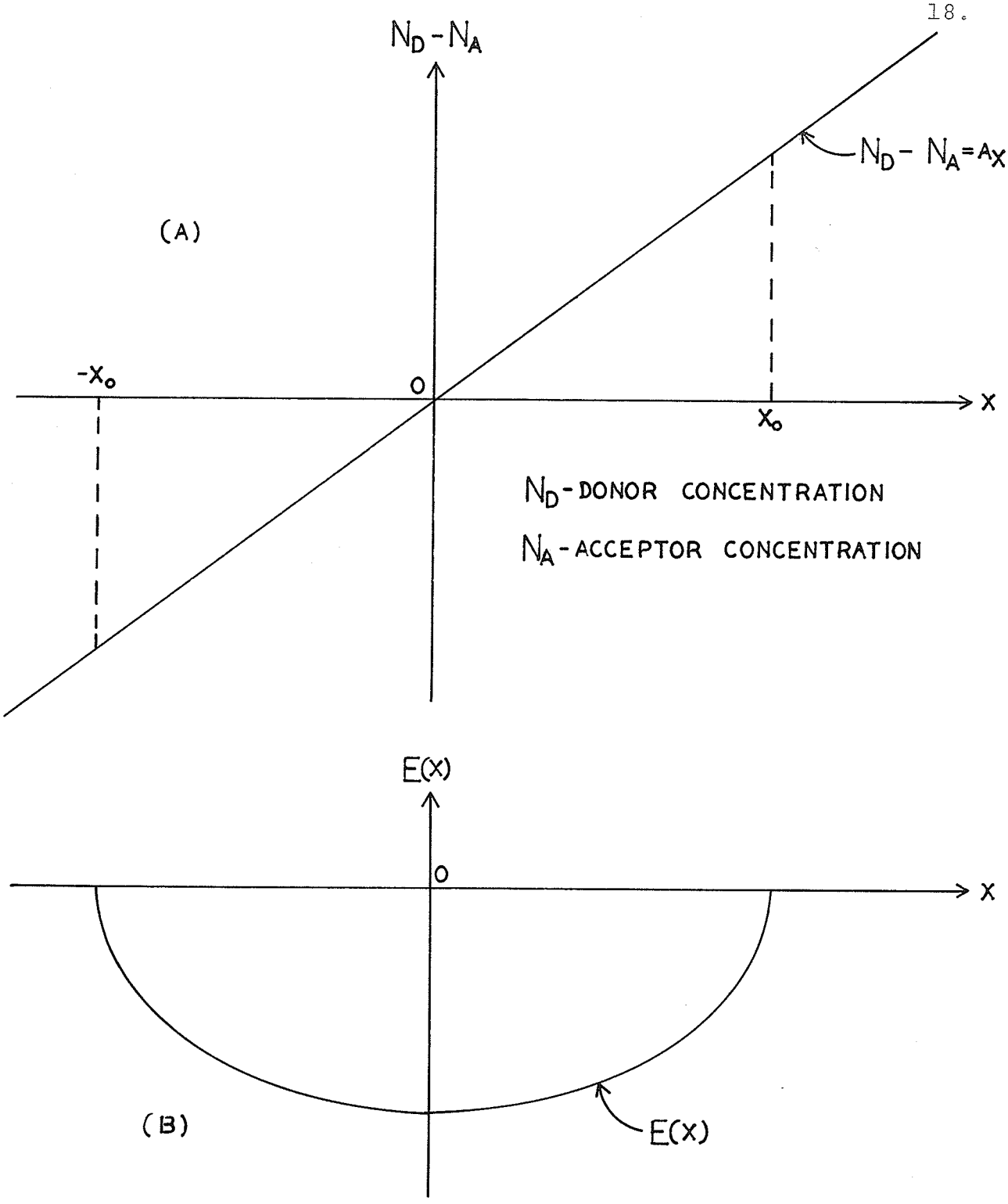

FIG. 2.3(A). IMPURITY DENSITY IN A LINEARLY GRADED JUNCTION.

(B) FIELD DISTRIBUTION IN A LINEARLY GRADED JUNCTION.

where $W_{eff} = W \int_o^1 \exp\left[-\frac{E^2}{1-E^2} \cdot \frac{b}{E_m}\right] dE$

$$\alpha_{max} = \alpha_\infty e^{-b/E_m}$$

The determination of the ionization integral for the graded junction is now identical to the determination of the ionization integral for the step junction except for details. At voltages less than the breakdown voltage the multiplications are

$$1 - \frac{1}{M_n} \simeq \frac{\ell_n \gamma}{\gamma - 1} \left(\frac{V}{V_B}\right)^{2/3(n+1)}$$

$$1 - \frac{1}{M_p} \simeq \frac{\gamma \ell_n \gamma}{\gamma - 1} \left(\frac{V}{V_B}\right)^{2/3(n+1)} \qquad \ldots(25)$$

The empirical result agrees with (25) approximately if $\alpha_p \simeq \alpha_n$ (γ close to unity) and $b/E_m >> 1$.

In the case where the ratio $\gamma (= \alpha_p/\alpha_n)$ is not constant, it is possible to make some estimates based on upper and lower limits. To calculate the breakdown voltage where M is infinite, we require

$$1 - \frac{1}{M_p} = \frac{\gamma}{1-\gamma} \left\{\exp\left[-(1 - \tfrac{1}{\gamma}) \int_o^W \alpha_p \, dx\right] - 1\right\} = 1 \qquad \ldots(26)$$

as well as

$$1 - \frac{1}{M_n} = \frac{1}{\gamma - 1} \left\{\exp\left[(\gamma - 1) \int_o^W \alpha_n \, dx\right] - 1\right\} \qquad \ldots(27)$$

At finite multiplications the calculation is closely approximated using the physical parameters of the incident carrier. For small multiplication, as in transistor collectors near

$\alpha M = 1$, the calculation for multiplication using the parameters for the incident carrier converges very closely to the true value. In all cases it is of the greatest importance to use the value of γ which is obtained at the maximum field.

CHAPTER III

MICROPLASMA PHENOMENON

3.1 REVIEW ON MICROPLASMA PHENOMENON

In avalanche breakdown the junction does not suddenly begin to conduct very large currents all over the junction, but rather at small discrete points. These small-high-current-density discharges are known as microplasmas. This effect indicates that breakdown occurs in small steps of current. Further increase in applied voltage beyond that which created the first microplasma would not increase the current through individual microplasma appreciably, but rather will produce more microplasmas. Each new microplasma adds its unit of current to the total breakdown value. The individual microplasma switches on and off in the area of initial breakdown, thus producing a distinct noise in the form of erratic current pulses with very fast rise time and of rather uniform amplitude regardless of the level of the breakdown voltage.

Associated with the generation of microplasmas in avalanche breakdown of the junction, there exists an emission of light eminating from the individual microplasma as pin-pointed spots of light. It has been found that microplasmas occur preferentially along areas of scratches or other mechanical effects [39]. It seems to suggest an effect of lattice damage on the junction width, perhaps a sort of dislocation

within the junction.

The generation and decay of the microplasmas during junction breakdown takes place in a very short time interval (10^{-10} sec. or lower) and hence the breakdown effect may be used at rather high speeds.

In general it is believed that high field intensity at local avalanche breakdown is involved in production of microplasma. Experimental evidence indicated that microplasmas are caused by localized high field regions within the junction.

Shockley suggested a model for explaining the observed properties of microplasmas. According to his model, field enhancement is caused by precipitates of dielectrics. Traps in microplasma region tend to immobilize a high density of charges. These charges are able to increase the electric field to such a value that breakdown may occur and thus a 'lock on' mechanism is produced. Spherical dielectric precipitate is assumed and since the dielectric constant of the spherical precipitate is much lower than the surrounding material, the field around the periphery will be stronger than the surrounding. Thus high local field intensity results in breakdown. The precipitates are nucleated preferentially at dislocations and so microplasmas occur, in general, preferentially along dislocations.

The most significant electrical behaviour of microplasmas is the characteristic current instability at breakdown.

If the diode is operated with a low resistance in series, the microplasma passes current as square pulses. The length and repetition rate of the pulses fluctuate statistically around an average value corresponding to the DC current flowing through the microplasma region. The repetition rate varies for different microplasmas. From experimental results on large load resistance circuits, Champlin [5] suggested that microplasma is due to a local avalanche breakdown and that the noise pulse is due to charge and discharge of the capacitance across the microplasma region. When the bias voltage is increased, the capacitance is charged up and the voltage across the microplasma region is increased. At breakdown, the resistance of the microplasma spot decreases. The capacitance then discharges through the resistance to decrease the voltage across the microplasma spot. If the voltage is decreased to or below a certain value that the field intensity in the microplasma region is not strong enough to sustain avalanche breakdown, the conduction ceases. After this, the capacitance is then charged up again. Haitz [17] extended this model to explain microplasma phenomenon on small load resistance circuits.

Champlin [5] and McIntyre [31] have independently developed a phenomenological theory describing the statistics of microplasma pulses. According to Champlin the electrical properties of a random bistable microplasma can be qualitatively ascribed with three fundamental parameters: (i) the probability rate for transitions from the non-conducting state to the

conducting state, $\emptyset_{01}(V,T)$ sec^{-1} (or turn-on probability); (ii) the corresponding probability for the opposite transition $\emptyset_{10}(V,T)$ sec^{-1} (turn-off probability); (iii) the pulse current $I_1(V,T)$.

Turn-on probability is mainly determined by the number of minority carriers entering the microplasma region and generating a pulse. Thus it is possible to enhance the pulse rate by illuminating the junction. Turn-off probability depends only on current. An interesting property of microplasma is that even at very high current pulses corresponding to several hundred electrons and holes within the plasma, there is still a finite turn-off probability. A better understanding of the process causing avalanche breakdown might result from the fact that holes have much lower ionization rates than usually assumed. If the ionization rate of holes is much lower than that of the electrons, a large number of holes have to be present to produce one or two secondary electrons. Thus it may be possible to explain the high pulse currents. Since $\emptyset_{10}$, $\emptyset_{01}$ and $I_1(V,T)$ are functions of voltage, the terminal properties of a microplasma are not unique but depend on the impedance of the external circuit. For the case of an ideal low impedance connection, however, the voltage is time independent.

According to Champlin the breakdown voltage is defined in terms of turn-off probability $\emptyset_{10}$, by

$$\lim_{V \to V_b^+} \emptyset_{10} = \infty \qquad \ldots(1)$$

Experimentally it was found that $\emptyset_{10}$ is a monotonically decreasing function of V and traverses the entire bistable range from $\emptyset_{10} \to \infty$ (non-conducting) to $\emptyset_{10} \to 0$ (continuously conducting) as V traverses a tiny increment of voltage δV above the breakdown voltage V_b. Some breakdown regions are not bistable but can be classified as multistable.

For ideal low impedance circuit, Champlin [5] assumed that it is time-independent. Let average times spent in the non-conducting and conducting states be τ_o and τ_1, respectively.

$$\tau_0 = \frac{1}{\emptyset_{01}} \qquad \ldots(2)$$

$$\tau_1 = \frac{1}{\emptyset_{10}} \qquad \ldots(3)$$

The pulse repetition rate N and the average current I are written as

$$N = \frac{\emptyset_{10}\,\emptyset_{01}}{\emptyset_{10}+\emptyset_{01}} \qquad \ldots(4)$$

$$I = \frac{\emptyset_{01}}{\emptyset_{10}+\emptyset_{01}} I_1 \qquad \ldots(5)$$

or in terms of the "off" and "on" times.

$$N = (\tau_0 + \tau_1)^{-1} \qquad \ldots(6)$$

$$I = \frac{\tau_1}{\tau_0 + \tau_1} I_1 \qquad \ldots(7)$$

where τ_1 is a very sensitive monotonically increasing function of V.

Eliminating τ_1 from (6) and (7), we have

$$N = \left(\frac{1}{\tau_0}\right)(1 - I/I_1) \quad \text{for} \quad 0 \leq I/I_1 \leq 1 \qquad \ldots(8)$$

Obviously the pulse rate is approximately $1/\tau_0$ at low current and approaches zero as I/I_1 approaches unity. The small signal AC conductance is the slope of average current verses applied voltage curve.

$$g = \frac{\partial I}{\partial V} = \frac{\partial I}{\partial \emptyset_{01}} \frac{\partial \emptyset_{01}}{\partial V} + \frac{\partial I}{\partial \emptyset_{10}} \frac{\partial \emptyset_{10}}{\partial V} + \frac{\partial I}{\partial I_1} \frac{\partial I_1}{\partial V} \qquad \ldots(9)$$

Conductance is only defined for low frequencies such that

$$f << (\emptyset_{01} + \emptyset_{10}) \qquad \ldots(10)$$

Spectral density of current fluctuations is $S_i(f)$

$$\langle \Delta i^2 \rangle = \int_0^\infty S_i(f)\, df \qquad \ldots(11)$$

where Δi is the deviation of the current from the average value. The current spectral density was shown to be

$$S_i(f) = 4 I_1^2 \frac{\tau_o \tau_1}{(\tau_0 + \tau_1)^2} \frac{\tau}{(1 + \omega^2 \tau^2)} \qquad \ldots(12)$$

where

$$\frac{1}{\tau} = \frac{1}{\tau_0} + \frac{1}{\tau_1} \qquad \ldots(13)$$

by Champlin [5]. This spectrum has $(1 + \omega^2\tau^2)$ frequency dependence which is characteristic of a Markoff process, with correlation time .

Eliminating τ_1 from (12) by using (7), the spectral density is

$$S_i(f) = 4 \tau_0 I_1^2 (I/I_1)^2 (1-I/I_1) \cdot \{1+(\omega\tau_0)^2 (I/I_1)^2\}^{-1}, 0 \leq I \leq I_1 \qquad \ldots(14)$$

At low frequencies ($\omega\tau_0 << 1$) this becomes

$$S_{io}/4\ \tau_0 I_1^2 = (I/I_1)^2\ (I - I/I_1) \qquad ...(15)$$

The noise maximum is proportional to the average "off" time and to the square of the pulse magnitude.

From Champlin's analysis of random, bistable element in an ideal high impedance circuit the process is not Markoffian. The noise is not simply related to the noise at low impedance. The field dependence of the initiation of breakdown suggests that field emitted carriers are involved. According to Champlin [5], the turn-off probability $\emptyset_{10}(V)$ was assumed to be single-valued and traverses the bistable range $\infty \geq \emptyset_{10} \geq 0$ as V(t) traverses the increment of voltage between V_b and $V_b + \delta V$. The quantities I_1 and $\emptyset_{01}$ may also be voltage dependent to a lesser degree.

Circuit diagram for observing random voltage pulses is shown in Figure 3.1. The capacitance C represents the total parallel capacitance. One observes pulses of voltage which are randomly distributed in magnitude above V_b.

From Figure 3.2 at T = 0 an event occurs which causes the bistable element to change to the non-conducting state. The entire supply current flows through the capacitance C, thus the voltage rises at a constant rate dV/dt = (I/C). During this portion of the pulse there is a probability rate $\emptyset_{01}$ that the element will switch to the conducting state.

Magnitude of the pulse is

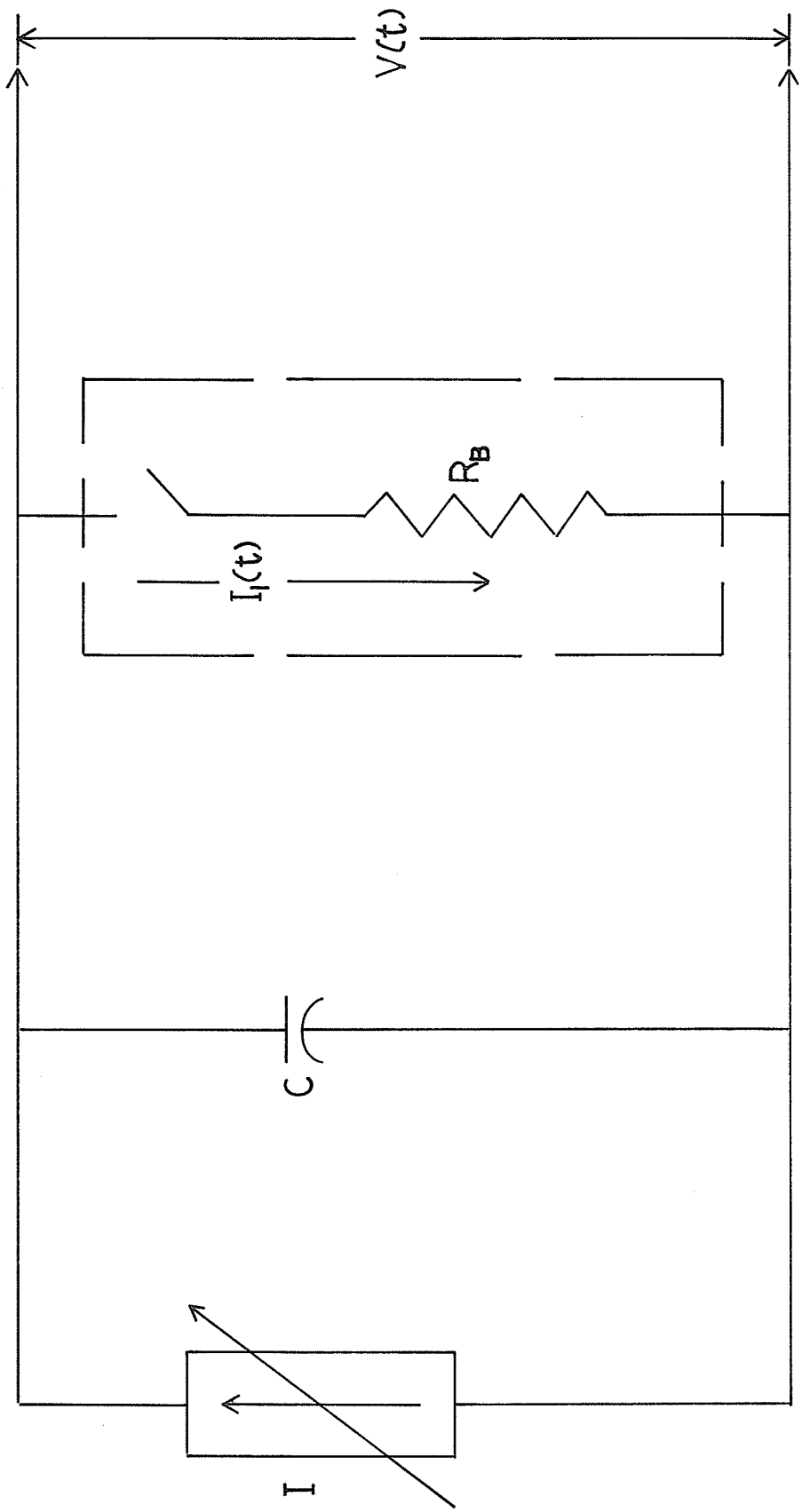

FIG. 3.1. CIRCUIT REPRESENTATION OF RANDOM VOLTAGE PULSE.

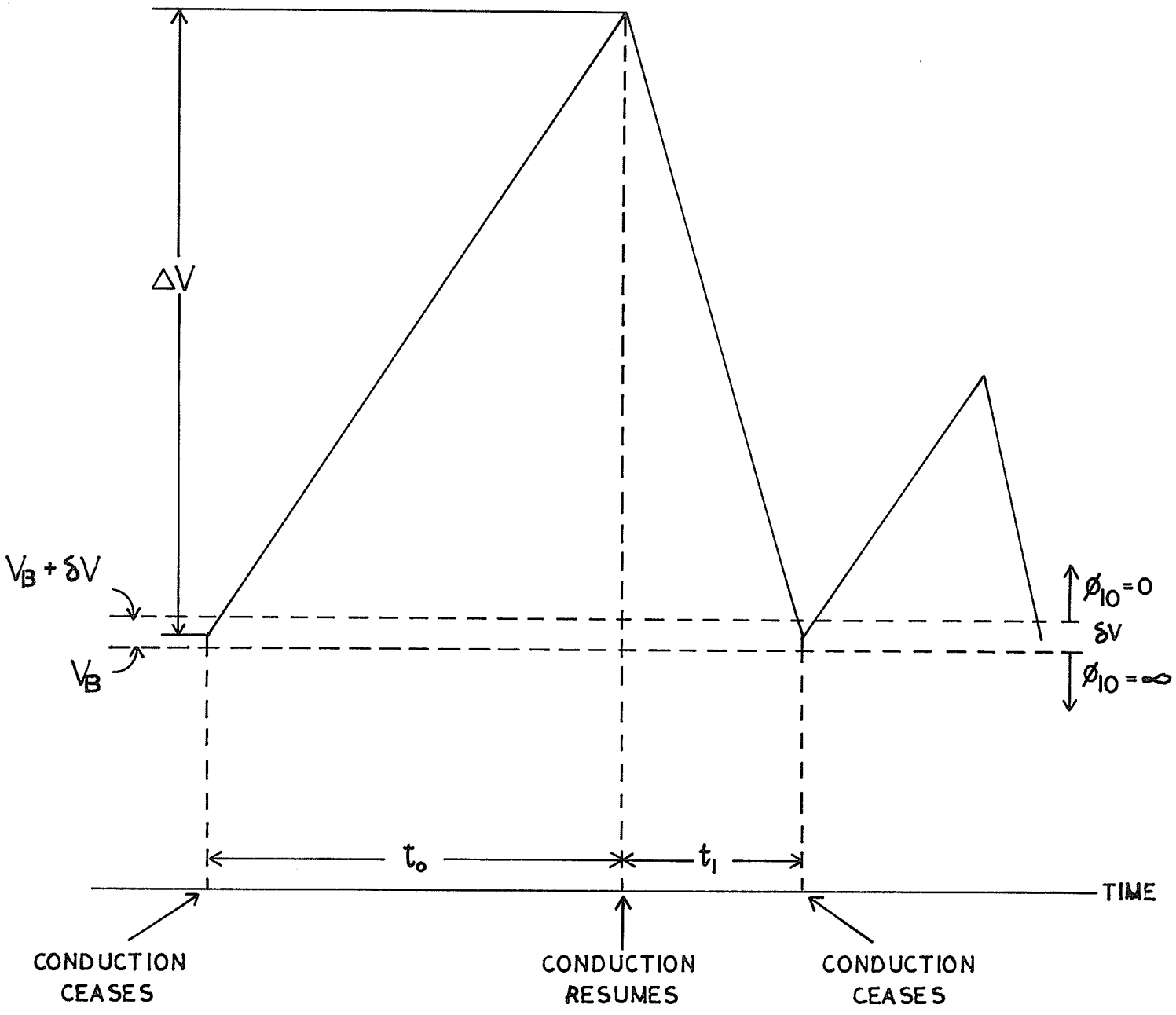

FIG. 3.2. FORMATION OF A VOLTAGE PULSE.

$$\Delta V = (I/C)t_o \qquad \ldots(16)$$

For $t>t_o$ the current $I_1(t)$ flows through a bistable element. Since $I_1(t) \geq I$ (the average current), the rate of change of capacitor voltage is negative.

$$\frac{dV}{dt} = \{I - I_1(t)\}/C \; ; \quad t_o<t \qquad \ldots(17)$$

In general, the current $I_1(t)$ varies with time as V(t) decreases. By assuming that $I_1(t) = I_{10}$, a constant, the voltage thus decreases at a constant rate:

$$\frac{dV}{dt} = \{I - I_{10}\}/C \; ; \quad t_o<t \qquad \ldots(18)$$

and continues to decrease until V(t) reaches the increment between V_b and $V_b + \delta V$. At some voltage in this range, conduction ceases and a new pulse begins. Assuming that this occurs at $t = t_o + t_1$ sec., the voltage drop during the second portion of the pulse is

$$\Delta V' = [(I_{10} - I) / C]\, t_1 \qquad \ldots(19)$$

For $\delta V << \Delta V$, the voltage rise and voltage drop may be equated.

$$t_1 = [I/\{I_{10} - I\}] \quad t_o \qquad \ldots(20)$$

Thus the "on" time t_1 is determined by the "off" time t_o. Averaging equation (20) and rearranging yields

$$I_1 = \{\bar{t}_1/(\bar{t}_o + \bar{t}_1)\}\, I_{10} \; , \quad 0 \leq I_1 \leq I_{10} \qquad \ldots(21)$$

Since t_o has an exponential distribution, the pulse magnitude in this case is also exponentially distributed.

$$F(\Delta V)d(\Delta V) = (N/\langle\Delta V\rangle) \exp(-\Delta V/\langle\Delta V\rangle)d(\Delta V) \quad ...(22)$$

From experimental results, increasing the applied voltage increased the ratio of average "on" to "off" time but had little effect on the magnitude of the current pulse. It is significant that at a given operating point, the pulse magnitude was invariant. This would not have been the case if breakdown occurs in more than one region. Investigating this behaviour, we can say that this is due to a local breakdown region, i.e. exhibition of microplasma breakdown.

Haitz [20] proposed an improved model to describe the electrical behaviour of microplasmas. Three components were used to form a basis for microplasmas. They were:

(i) V_B breakdown voltage, a constant;

(ii) r_s series resistance, a constant;

(iii) $f(\emptyset_{10})$ a continuous function depending on the turn-off probability on current.

The breakdown voltage V_B can be determined in two ways:

(i) by extrapolation of 1/M to zero;

(ii) by extrapolation of the resistive part of the V-I characteristic to zero current.

Both values are equal within experimental accuracy. V_B is fixed by the condition that the field strength in the central part of the junction has to be equal to the breakdown field. If the applied voltage is raised above V_B, the voltage across the microplasma in the on-condition does not change appreciably because a very small increase of voltage causes an

enormous increase of current. Practically all of the voltage drop above V_B is across the series resistance. This series resistance is made up of two parts: (1) space charge resistance and, (2) spreading resistance from the microplasma.

The space charge resistance, as shown by Shockley [51], is a consequence of the motion of carriers of one sign going through the outer parts of the depletion layer and setting up a field that tends to reduce the field in the centre part of the junction giving rise to an effective resistance R_{sc}.

$$R_{sc} = (W^2/A)\ (\tfrac{1}{3}\ K\ V_d) \quad \text{ohms} \qquad \ldots(23)$$

where W = depletion layer width

A = area of microplasma

K = dielectric constant

V_d = limiting drift velocity

In most practical junctions, one side of the junction has a very low resistivity, and so the spreading into the higher resistivity part has to be considered. The spreading resistance from the microplasma is given by

$$R_{sp} = S/2D \qquad \ldots(24)$$

where D = diameter of microplasma

S = resistivity .

In most cases, the contribution from the space charge resistance is higher than that from the spreading resistance.

In Haitz's model each point along the resistive part is associated with a turn-off probability. In the neighbourhood

of V_B the pulses are extremely short. Since V_B cannot be measured accurately, it has to be extrapolated.

The relaxation phenomenon from traps is also an important event in the production of microplasmas. Pulse groups were observed by Haitz [19] when microplasmas were operated at low temperatures. This can be explained by the fact that traps in microplasmas are charged during one pulse and then causing subsequent pulses by release of carriers. The turn-on probability $\emptyset_{01}$ drops sharply with the time elapsed after the last pulse was experimentally justified by Haitz. Obviously charge is leaked from the traps, and thus reducing the turn-on probability $\emptyset_{01}$. At room temperature, these effects cannot be clearly observed because there are more thermal carrier initiating pulse. Naturally the trap density varies considerably from one microplasma to another, which accounts for the difference of turn-on probability that there are more pulses observed than thermal carrier passing through the microplasma is resolved by assuming the presence of traps.

Traps are also responsible for the interaction between different microplasmas that has been observed by Haitz [17] and Ruge [18]. If there are several microplasmas with about the same breakdown voltage, then all the microplasma 'turn-on' probability will be increased if one of the microplasma is in the 'on-condition'. When a voltage pulse is of sufficient amplitude so as to turn-on all the microplasmas, and after its application, nothing will happen after a certain time interval.

As soon as the first microplasma is on, all the others follow after a very short time compared to the waiting time until the first one occurred. This interaction takes place over a distance of more than 100μ. The cause of this interaction is not known. It may be caused by the release of carriers from traps by infrared light or phonons emitted from conducting microplasmas. Another possibility is the back scattering of hot carriers, which are then reaching other microplasmas.

3.2 MICROPLASMA IN SPACE-CHARGE-LIMITED SOLID-STATE DIODE

If an insulator or intrinsic semi-conductor is provided with an injecting contact on one side, and a collecting contact on the other, then space charge neutrality cannot be maintained in the insulator region. The current flowing through the device is space-charge limited. If one electrode injects holes into the organic semi-conductor and the other contact is non-injecting, there will be hole flow from the injecting contact to the non-injecting contact. Similar to the p-n junction diode, the space-charge-limited diode now has the p-region providing a hole-injecting contact and the n-region providing a hole-collecting contact. The anthracene diode made in this way is a single hole injection space-charge-limited diode.

In general, space-charge-limited currents depend only on the transport and trapping of the carriers within the

crystal. With given ohmic contacts, the current voltage relationship of an organic semiconductor is linear at low fields, but it becomes non-ohmic at higher values of the applied field. The causes are:

(a) space charge is formed as a consequence of large concentration of charge carriers between the electrodes at high current densities;

(b) existence of traps causes nonlinearity in the I-V curve.

Together with Hsu, an attempt is made to set up a model for explaining the microplasma breakdown in space-charge-limited solid-state diodes. The model is based on the discussions on avalanche breakdown and the microplasma phenomenon in the previous sections in conjunction with the characteristic of space-charge-limited diodes. The proposed model is shown in Figure 3.3. It is assumed that if the temperature of the lattice increases, the thermal scattering cross-section increases and the ionization probability decreases. All the energy of the ionized carrier is dissipated near or very near the microplasma. Therefore the temperature of the microplasma region will be considerably higher than that of the rest of the diode which in turn, will become warmer than its ambient after sufficient time.

In Figure 3.3, the series combination of R_1, R_2 and R is the DC resistance of the diode. R_1 is the ohmic contact.and also the resistance near the anode region. R is

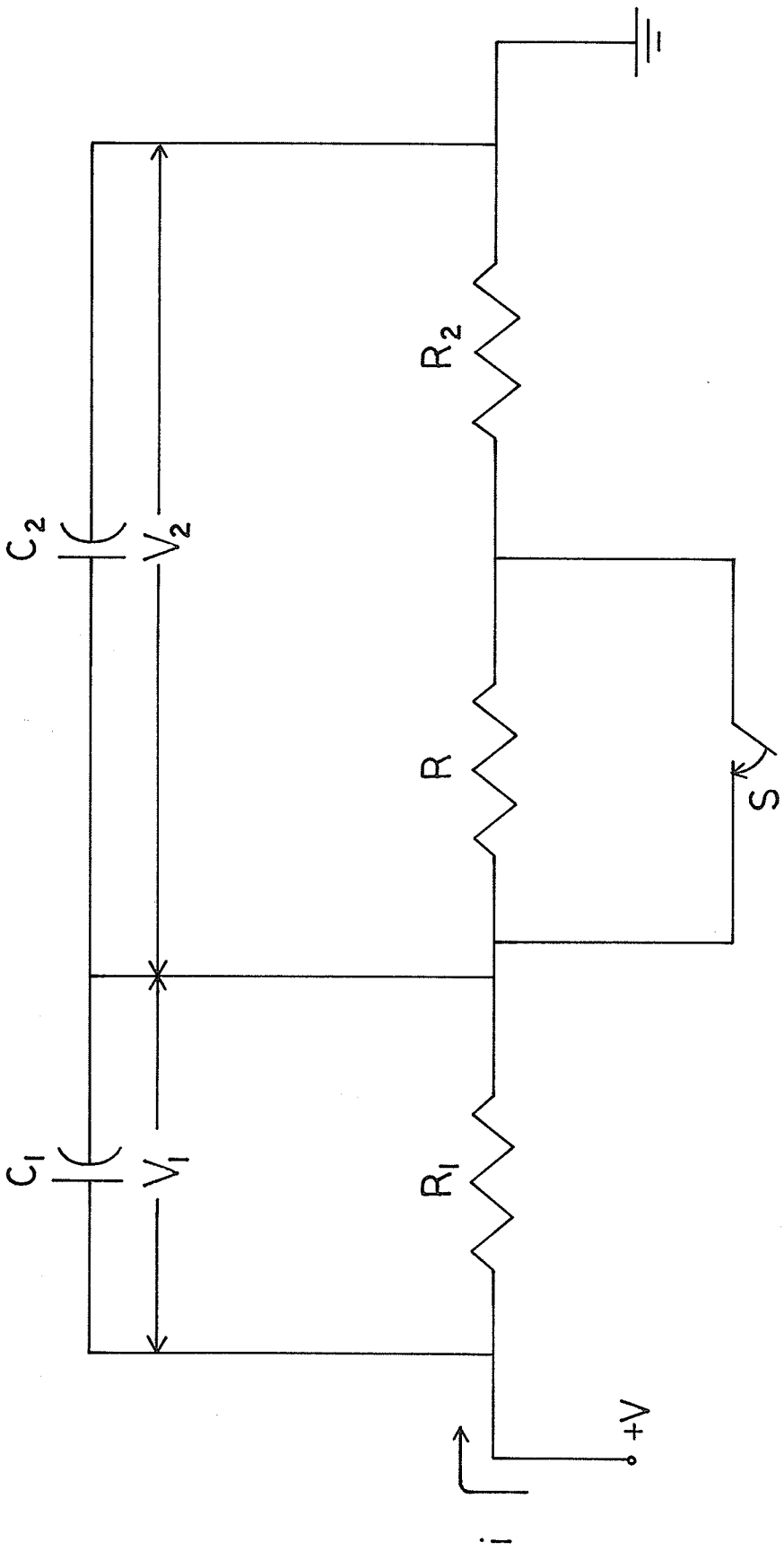

FIG. 3.3. EQUIVALENT CIRCUIT OF ANTHRACENE DIODE DURING MICROPLASMA BREAKDOWN.

the space charge resistance and R_2 is the spreading resistance. Their significance has already been explained in the previous section. The capacitance C_1 is the capacitance in the immediate neighbourhood of the anode since the injected charge is immediately localized in the neighbourhood of the electrode. The capacitance C_2 is a combination of capacitive effects due to both space charge and trap effects as explained earlier in this section.

The switch S is parallel to the space charge resistance R. This switch is essential for the turn-on or turn-off of microplasma when the resistance decreases or increases correspondingly. In general, the space charge resistance R is very large as compared to the spreading resistance and the ohmic contact resistance.

R will be in the mega-ohm range while the spreading and ohm contact resistances will be in the kilo-ohm range. The space charge capacitance C_2 is also comparatively larger than the localized contact capacitance C_1 because C_1 is only localized near the contact while the space charge capacitance C_2 is a bulk effect. For a 0.01 mm. thick anthracene crystal, the space charge capacitance C_2 will be in the pico-farad range.

The voltage and current characteristics of the circuit can be separated into two cases. Case (1) is when the microplasma is switched to non-conducting state represented

by Figure 3.4. Case (2) is when the microplasma is switched to conducting state represented by Figure 3.5. Their physical significances are explained analytically in the following section.

3.3 MATHEMATICAL ANALYSIS

3.3.1. Case 1 - Response Calculation as Switch is Off

$t < 0$, switch is on - steady state acquired

$t > 0$, switch is off

Initial conditions:

$$v_1(0_-) = \frac{R_1}{R_1 + R_2} \quad v$$

$$v_2(0_-) = \frac{R_2}{R_1 + R_2} \quad v$$

KVL: $$v_1 + v_2 = v \qquad \ldots(1)$$

KCL: $$ic_1 + i_{R1} = i_{C2} + i_{R2} = i \qquad \ldots(2)$$

From (2), $$C_1 \frac{dv_1}{dt} + \frac{v_1}{R_1} = C_2 \frac{dv_2}{dt} + \frac{v_2}{R_2 + R}$$

Taking Laplace Transform of (2),

$$C_1[SV_1 - v_1(0_-)] + \frac{v_1}{R_1} = C_2 [SV_2 - v_2(0_-)] + \frac{v_2}{R_T} \qquad \ldots(3)$$

where $R_T = R_2 + R$

Taking Laplace Transform of (1),

$$V_1 + V_2 = \frac{V}{S}$$

$$V_2 = \frac{V}{S} - V_1 \qquad \ldots(4)$$

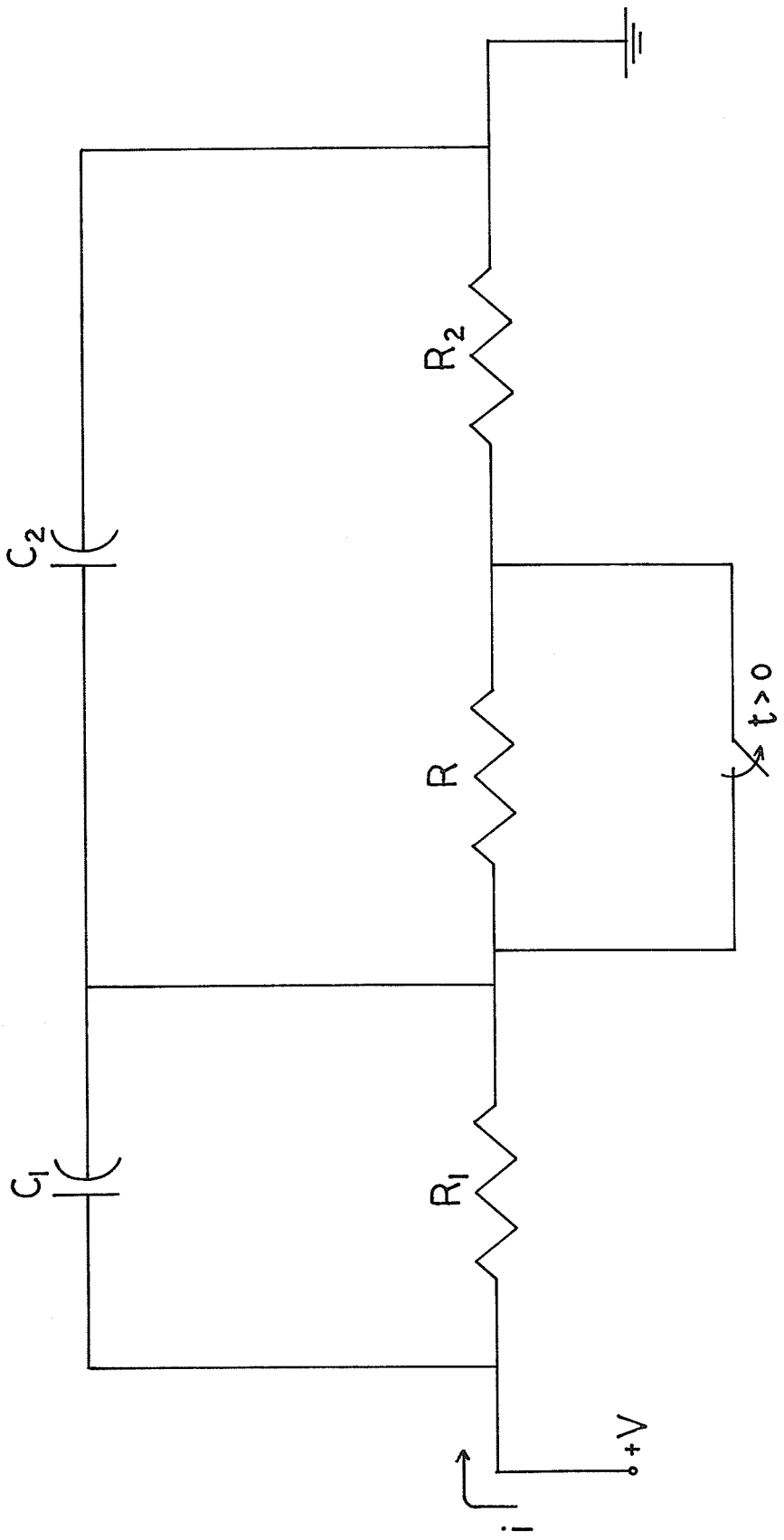

FIG. 3.4. CASE(i), SWITCH OPENED AT t>0 AFTER CLOSING FOR A LONG TIME.

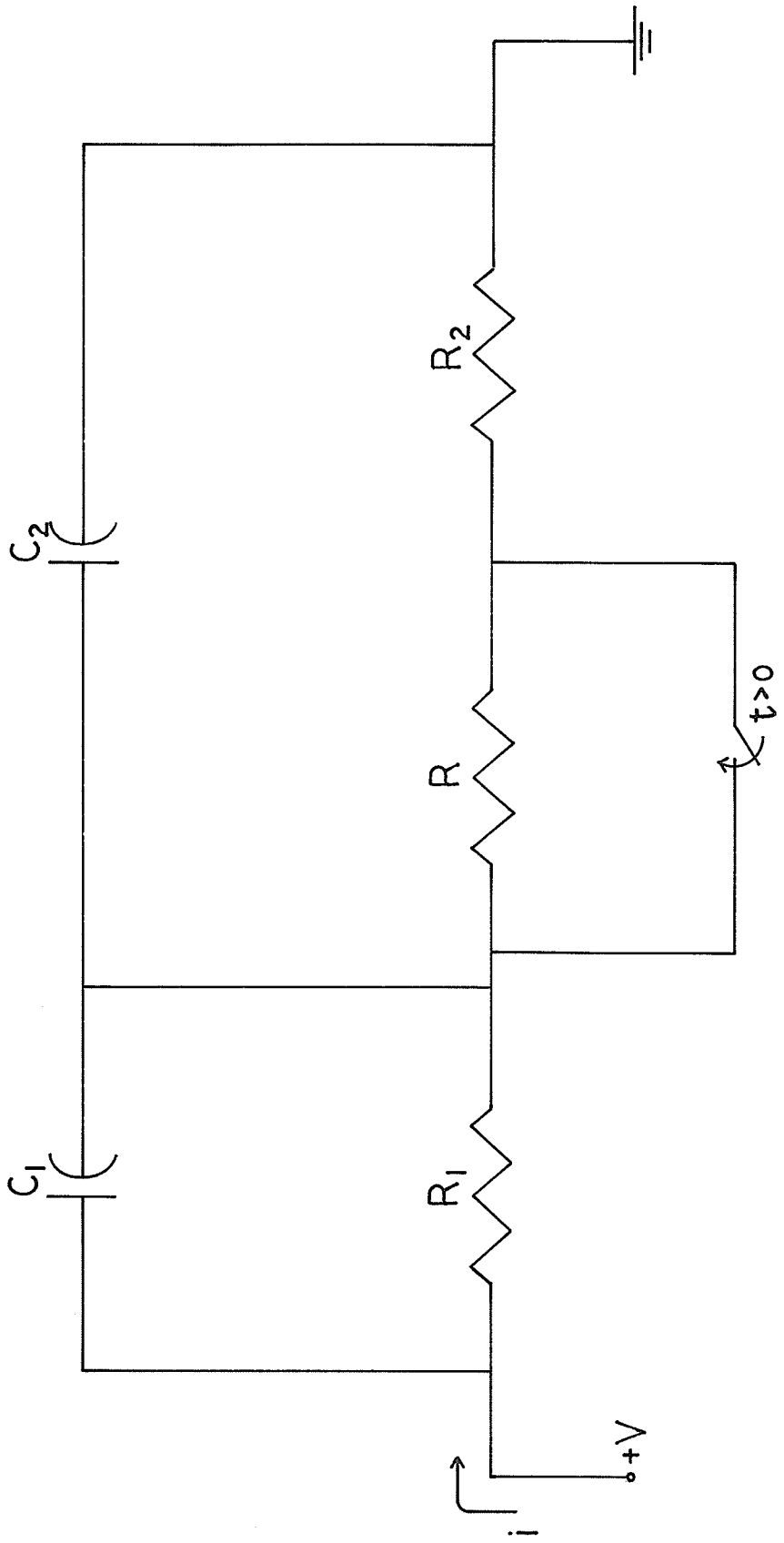

FIG. 3.5. CASE(ii), SWITCH CLOSED AT $t \geq 0$ AFTER OPENING FOR A LONG TIME.

From (3) and (4),

$$V_1 = \frac{Cv_1(0_-) - C_2v_2(0_-)}{(C_1+C_2)\,S + (\frac{1}{R_1}+\frac{1}{R_T})} + \frac{C_2S + G_T}{(C_1+C_2)\,S + (\frac{1}{R_1}+\frac{1}{R_T})} \cdot \frac{V}{S}$$

$$= \frac{C_1v_1(0_-) - C_2v_2(0_-)}{C_TS + G} + \frac{C_2S + G_T}{C_TS + G} \cdot \frac{V}{S} \qquad \ldots(5)$$

where $C_T = C_1+C_2$, $G = (R_1//R_T)^{-1}$, $G_T = \frac{1}{R_T}$

$$\therefore \quad I_{R_1} = \frac{G_1[C_1v_1(0_-) - C_2v_2(0_-) + \frac{V}{S}(C_2S + G_T)]}{C_TS + G} \qquad \ldots(6)$$

where

$$G_1 = \frac{1}{R_1}, \quad v_1 = v_1(0_-), \quad v_2 = v_2(0_-)$$

$$I_{C_1} = \frac{(C_1C_2S + C_1/G_T)\,V - C_1C_2(v_1+v_2)\,S - C_1Gv_1}{C_TS + G} \qquad \ldots(7)$$

Let,

Laplace Transform of equation (2) is

$$I = I_{R_1} + I_{C_1}$$

$$= \frac{C_1C_2(V - v_1-v_2)\,S + G_TG_1\frac{V}{S} + [C_1(G_TV - Gv_1) + G_1(C_2V+C_1v_1-C_2v_2)]}{C_TS + G}$$

$$= \frac{(C_1G_T + C_2G_1)\,V - C_1G_Tv_1 - C_2G_1v_2}{C_TS + G} + \frac{G_TG_1V}{C_T} \cdot \frac{1}{S(S + G/C_T)}$$

$$= \frac{(C_1G_T + C_2G_1)\,V - C_1G_T\,v_1 - C_2G_1v_2}{C_TS + G} + \frac{G_TG_1\,V}{C_T}\,C_T$$

$$\cdot \left(\frac{1}{S} - \frac{1}{S + G/C_T}\right)$$

$$I = \frac{\left(\frac{C_1}{R_T} + \frac{C_2}{R_1}\right) V - \frac{C_1}{R_T} V_1 - \frac{C_2}{R_1} V_2}{(C_1 + C_2)(S + 1/\tau)} + \frac{V}{R_1 + R_T}\left(\frac{1}{S} - \frac{1}{S + 1/\tau}\right)$$

where $\tau = \dfrac{R_1 R_T (C_1 + C_2)}{R_1 + R_T}$ is the time constant

$$\therefore \quad i(t) = \frac{\left(\frac{C_1}{R_T} + \frac{C_2}{R_1}\right) V - \frac{C_1}{R_T} V_1 - \frac{C_2}{R_1} V_2}{C_1 + C_2} \; e^{-t/\tau}$$

$$+ \frac{V}{R_1 + R_T}\left(1 - e^{-t/\tau}\right)$$

$$\text{i.e.} \quad i(t) = \frac{V}{R_1 + R_T} + e^{-t/\tau} \left[\frac{\left(\frac{C_1}{R_T} + \frac{C_2}{R_1}\right) V - \frac{C_1}{R_T} V_1 - \frac{C_2}{R_1} V_2}{C_1 + C_2} - \frac{V}{R_1 + R_T}\right] \qquad \ldots(8)$$

From initial conditions

$$v_1 = \frac{R_1}{R_1 + R_2} v$$

$$v_2 = \frac{R_2}{R_1 + R_2} v$$

$$i(t) = \frac{V}{R + R_1 + R_2} + \frac{V}{C_1 + C_2}\left[\frac{C_1}{R_T} + \frac{C_2}{R_1} - \frac{C_1}{R_T}\frac{R_1}{(R_1 + R_2)} - \frac{C_2}{R_1}\frac{R_2}{(R_1 + R_2)} - \frac{C_2}{R_1}\frac{R_2}{(R_1 + R_2)} - \frac{1}{R_1 + R_T}\right] e^{-t/\tau}$$

$$= \frac{V}{R_1 + R_2 + R} + \frac{V}{C_1 + C_2}\left[C_1 \frac{R_2}{R_T(R_1 + R_2)} + C_2 \frac{R_1}{R_1(R_1 + R_2)} - \frac{C_2}{R_1 + R_T}\right] e^{-t/\tau}$$

$$\therefore \quad i(t) = \frac{V}{R_1+R_2+R} + \frac{V\,[C_2R(R+R_2) - CRR_1]}{(C_1+C_2)(R+R_2)(R_1R_2)(R_1+R+R_2)}\, e^{-t/\tau} \quad ...(9)$$

In general, equation (9) can be written as

$$i(t) = \frac{V}{R_1+R_2+R}\,(1 - e^{-t/\tau}) + V\left[\frac{1}{R_1+R_2} - \frac{C_1R/(C_1+C_2)}{(R_1+R_2)(R+R_2)}\right] e^{-t/\tau}$$

or

$$i(t) = I(\infty)\,(1 - e^{-t/\tau}) + I(0_-)\left[1 - \frac{C_1R}{(C_1+C_2)(R+R_2)}\right] e^{-t/\tau} \quad ...(10)$$

where

$$I(\infty) = \frac{V}{R_1 + R_2 + R}$$

$$I(0_-) = \frac{V}{R_1 + R_2}$$

The current response characteristic is shown in Figure 3.6.

3.3.2 Case 2 - Response Calculation When Switch is On

The circuit diagram for this case is represented by Figure 3.5. The switch is turned on at t = 0. The initial conditions are

$$v_1(0_-) = \frac{R}{R_1 + R_2 + R}\, v$$

$$v_2(0_-) = \frac{R_2 + R}{R_1 + R_2 + R}\, v$$

$$R_T = R_2$$

Substituting the above values into equation (8)

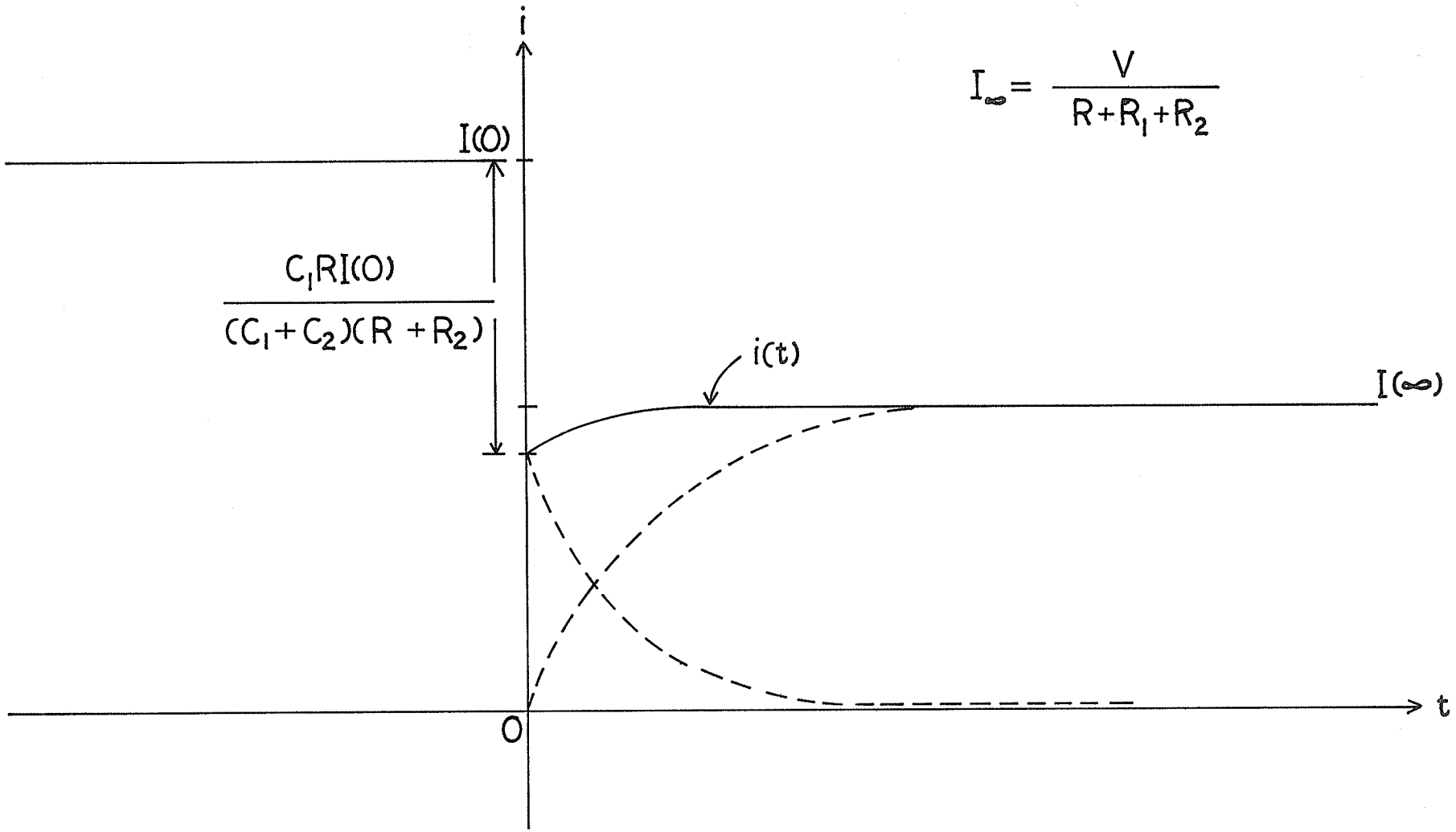

FIG. 3.6. CURRENT RESPONSE WHEN SWITCH IS OPENED AFTER CLOSING FOR A LONG TIME.

$$i(t) = \frac{V}{R_1+R_2} + \frac{V}{C_1+C_2}\left[\frac{C_1}{R_2}\left(1 - \frac{R_1}{R_1+R_2+R}\right) + \frac{C_2}{R_1}\left(1 - \frac{R_2+R}{R_1+R+R_2}\right) - \frac{C_1+C_2}{R_1+R_2}\right] e^{-t/\tau}$$

$$= \frac{V}{R_1+R_2} + \frac{V}{C_1+C_2}\left[\frac{C_1(R_2+R)}{R_2(R_1+R+R_2)} + \frac{C_2R_1}{R_1(R_1+R_2+R)} - \frac{C_1+C_2}{R_1+R_2}\right] e^{-t/\tau}$$

$$\therefore\ i(t) = \frac{V}{R_1+R_2} + \frac{V(C_1R - C_2R)}{(C_1+C_2)R_2(R_1+R_2)(R_1+R_2+R)} e^{-t/\tau} \qquad \ldots(11)$$

In general, equation (11) can be rewritten as

$$i(t) = \frac{V}{R_1+R_2}(1 - e^{-t/\tau}) + V\left[\frac{1}{R_1+R+R_2} + \frac{C_1R}{(C_1+C_2)R_2(R_1+R_2+R)}\right] \cdot e^{-t/\tau}$$

$$= I(\infty)(1 - e^{-t/\tau}) + I(0_-)\left[1 + \frac{C_1R}{(C_1+C_2)R_2}\right] e^{-t/\tau} \qquad \ldots(12)$$

where

$$I(\infty) = \frac{V}{R_1 + R_2}$$

$$I(0_-) = \frac{V}{R_1 + R_2 + R}$$

The current response for the 'on' case is shown in Figure 3.7.

Since the output current of the diode under both turn-on and turn-off condition is the sum of two terms, the time constant of the current pulses actually observed can be much larger than the RC time constant associated with the circuit.

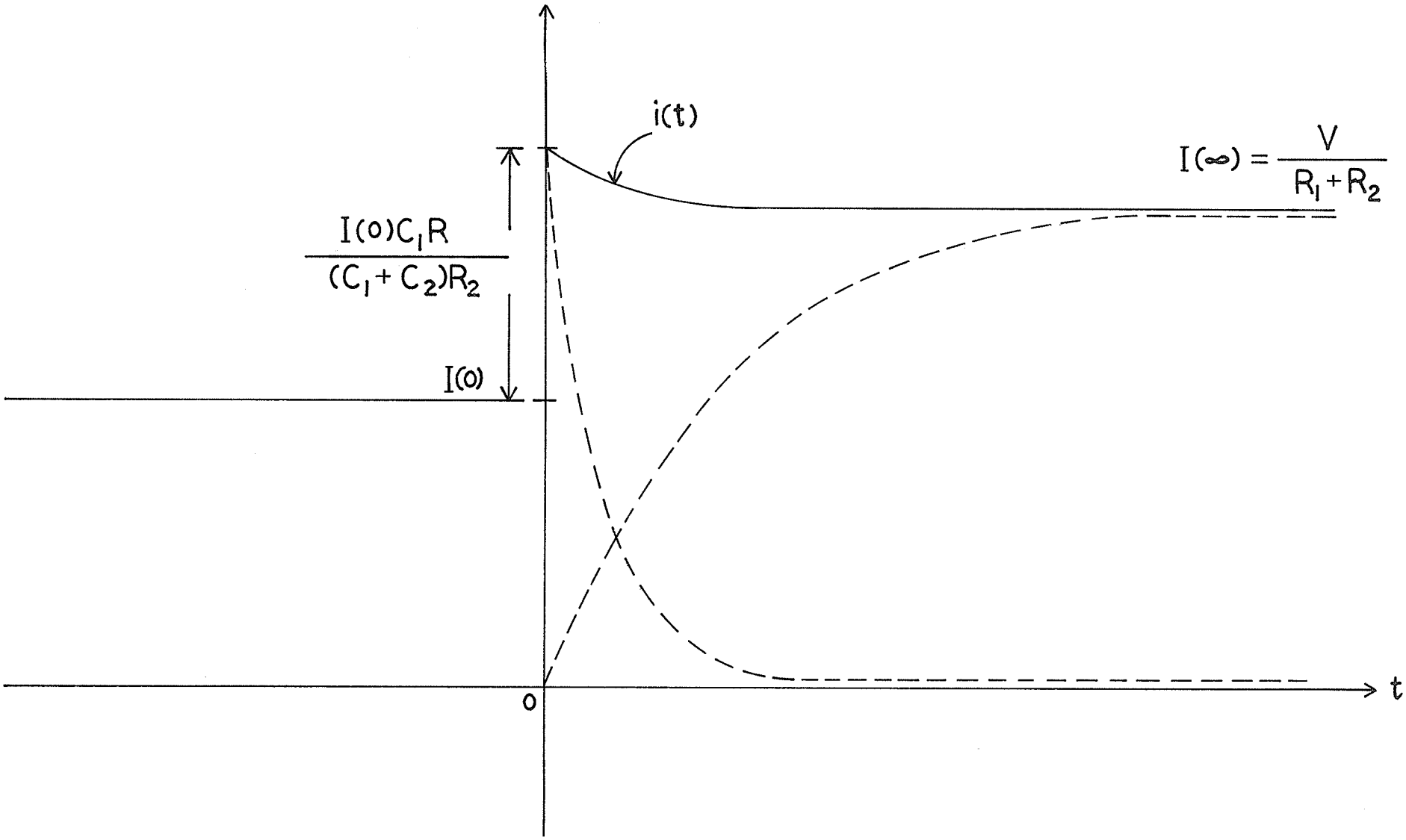

FIG. 3.7. CURRENT RESPONSE WHEN SW-ITCH IS CLOSED AFTER OPENING FOR A LONG TIME.

3.4 USING MICROPLASMA TO MEASURE TEMPERATURE COEFFICIENT OF THE AVALANCHE BREAKDOWN VOLTAGE

The breakdown voltage of an avalanche diode varies with temperature. The temperature changes may be due to internal heating effects caused by power dissipation or to a change in the ambient temperature. Avalanche breakdown exhibits a positive temperature coefficient.

In general, temperature coefficient may be defined as

$$K_T = \frac{\Delta V_B}{\Delta T} \frac{mv}{^oC} \qquad ...(13)$$

where ΔV_B is the change in breakdown voltage corresponding to the change in temperature ΔT. As the breakdown voltage depends on temperature, we have

$$V_B(T) = V_B(T_o) \, [1 + \beta(T - T_o)] \qquad ...(14)$$

where T_o is the room temperature.

The temperature coefficient can thus be calculated as

$$\beta = \frac{V_B(T) - V_B(T_o)}{T - T_o} \qquad ...(15)$$

The reverse current-voltage characteristics of a modern p-n junction has a sharp change in slope indicating the breakdown of the junction. Thus the breakdown voltage of a modern p-n junction can be accurately determined from its reverse I-V characteristic. However, for space-charge-limited solid-state diodes the breakdown voltage cannot be accurately observed since there is no sharp increase in current. An alternative method has to be used to measure the breakdown voltage.

As it was previously described, the microplasma is due to a local breakdown phenomenon. Consequently the microplasma phenomenon can be used to measure the breakdown characteristic of a soft junction or a space-charge-limited solid-state diode. Although the microplasma breakdown occurs at a voltage lower than the actual junction breakdown, (the onset of microplasma breakdown cannot be used as the onset of the junction breakdown), the temperature coefficient of the breakdown voltage of the device and that of the onset of the microplasma breakdown should be exactly the same. The microplasma can, therefore, be used to determine the temperature coefficient of the breakdown voltage in a solid-state device accurately. There are experimental devices by the author to support this statement.

The temperature coefficient of the breakdown voltage of a silicon p-n junction has been studied very extensively in the past. Chynoweth and McKay [10] has shown experimentally that the temperature coefficient of the avalanche multiplication constant M is always positive and actually independent of V_B. Data from experiments by Garside and Harvey [13] justified this statement.

Experiments on silicon p-n junction onset voltage of microplasma noise has been done by Hsu. Experimental data were plotted in Figure 5.1, Figure 5.2 and Figure 5.3, respectively. In order to verify our theory, we can compare the experimental data with the existing data.

This experiment showed that indeed the temperature

coefficient of the junction breakdown voltage and that of the onset voltage of microplasma are exactly the same. The discrepancy of the experimental results is presumably due to the doping concentration and the impurity profile of the junction.

CHAPTER IV

MEASUREMENT METHODS

4.1 EXPERIMENTAL METHODS - Sample Preparation

Since a p-n junction still cannot be formed in an anthracene crystal, the sample used in this experiment are conventional single-injection space-charge-limited diodes. The anthracene single crystal was cut along the ab plane and is etched to approximately 0.01 cm. thick. The solution used for etching was benzene. It was observed that the etching rate could be accelerated by warming up the solution to about 70°C.

After the etching procedure, the next step was to make ohmic contacts on the crystal. It is necessary to use low work function materials for ohmic contact in order to prevent inhibition of injection. A concentrated solution of sodium and anthracene in tetrahydrofuran in contact with the crystal were evaporated. The purpose served was to completely remove oxygen, water vapor and materials which would interact with the contact solution. Sodium solution was chosen because the other alkali metals would not form a more stable contact. The crystal was then washed again in benzene solution. Silver paste was applied to both surfaces as electrodes. The silver-paste-anthracene contact is a hole injection electrode. No electron is injected into the sample. The area of the major surface of the crystal is larger than 0.5 x 0.5 cm^2. The area of the electrode is approximately equal to 1 mm^2.

4.2 EXPERIMENTAL PROCEDURE

4.2.1 Current-Voltage Characteristics

The current-voltage breakdown characteristics of the sample at various temperatures were observed with an oscilloscope (Tektronix type 502). The experimental set up was shown in Figure 4.1. The resistors and sample were mounted in a jig which was dovered up to keep light from reaching the sample. A thermometer was clamped in place between the power resistor and the sample so that the ambient temperature of the sample could be taken. The breakdown voltage and avalanche current were noted every 10°C rise of temperature.

4.2.2 Low Frequency Noise Measurement on Anthracene

The low frequency noise measurement set up is shown in Figure 4.2. The average circuit and the jig circuit are shown in Figure 4.3, and Figure 4.4, respectively.

Noise sampled from the measured specimen was passed through the preamplifier and then into wave analyzer. An average circuit was used to stabilize the signal for detection in the noise meter. A sinusoidal source was used as a calibrating signal.

The noise current equation is given as

$$\overline{i_o^2} = 2qI_{eq}\,\Delta f \qquad \ldots(1)$$

where $\overline{i_o^2}$ is the noise density

I_{eq} is the equivalent current to represent noise density

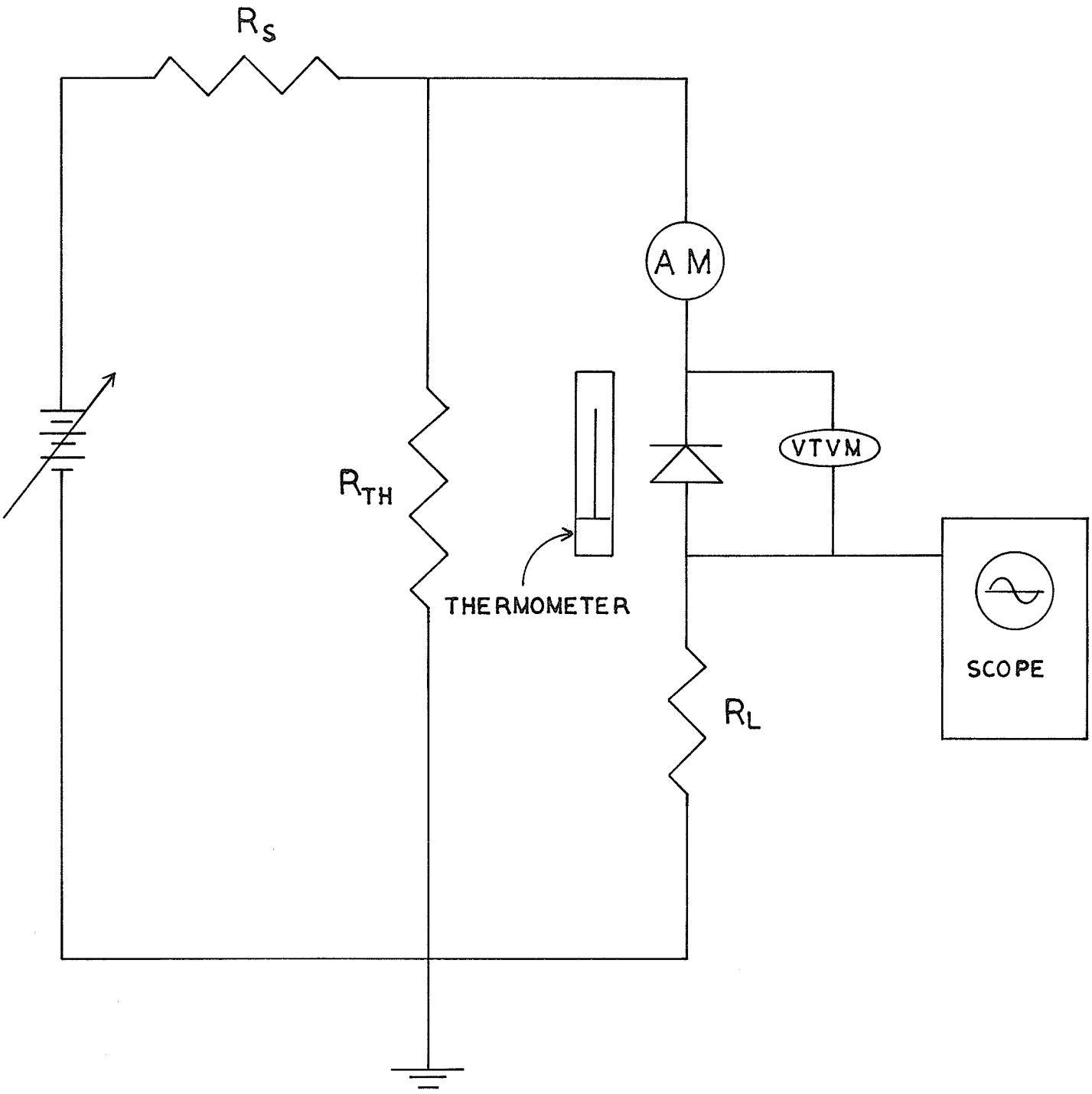

FIG. 4.1. EXPERIMENTAL SET-UP FOR MEASURING BREAKDOWN VOLTAGE AS A FUNCTION OF TEMPERATURE.

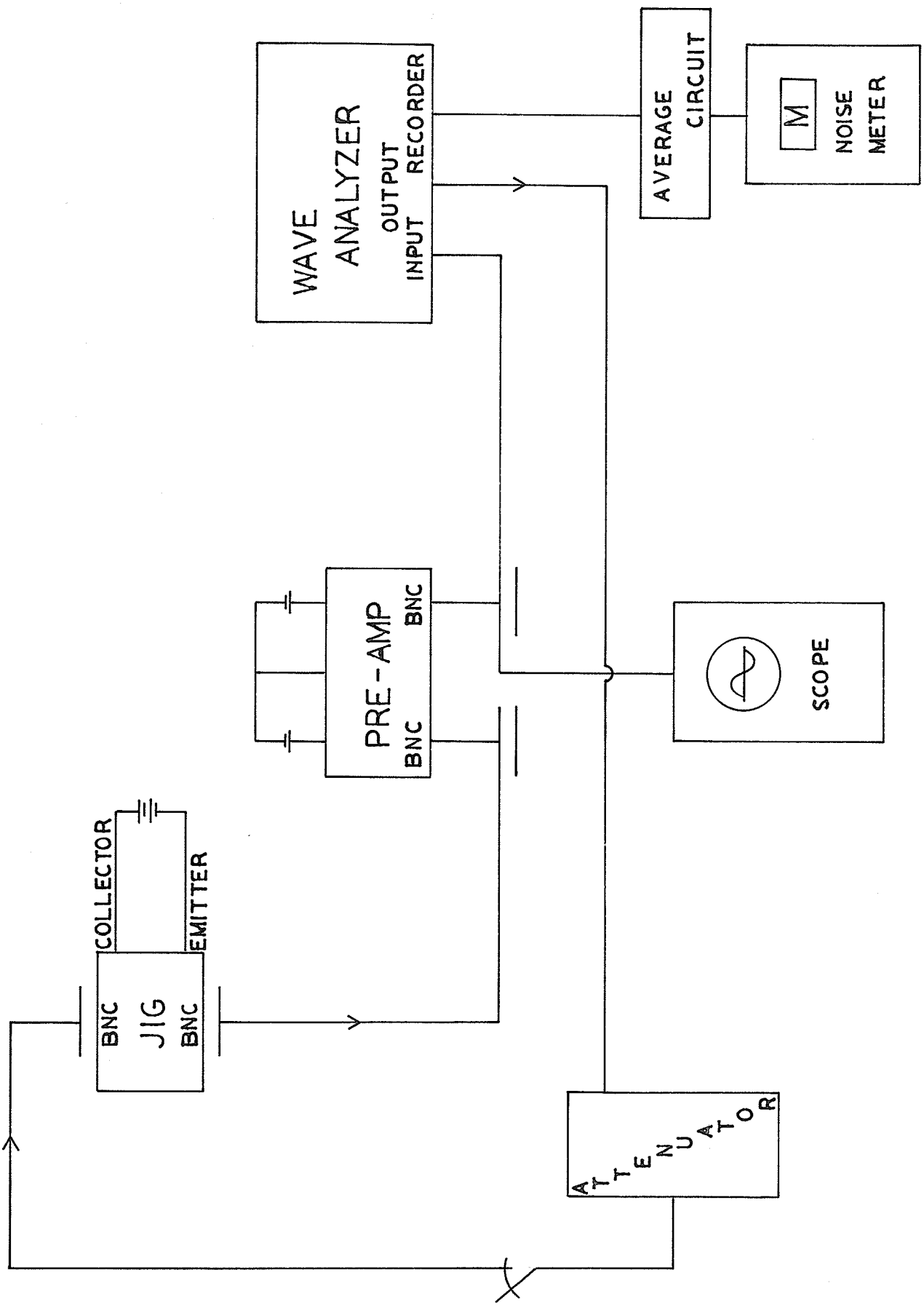

FIG. 4.2. LOW FREQUENCY NOISE MEASUREMENT SET-UP.

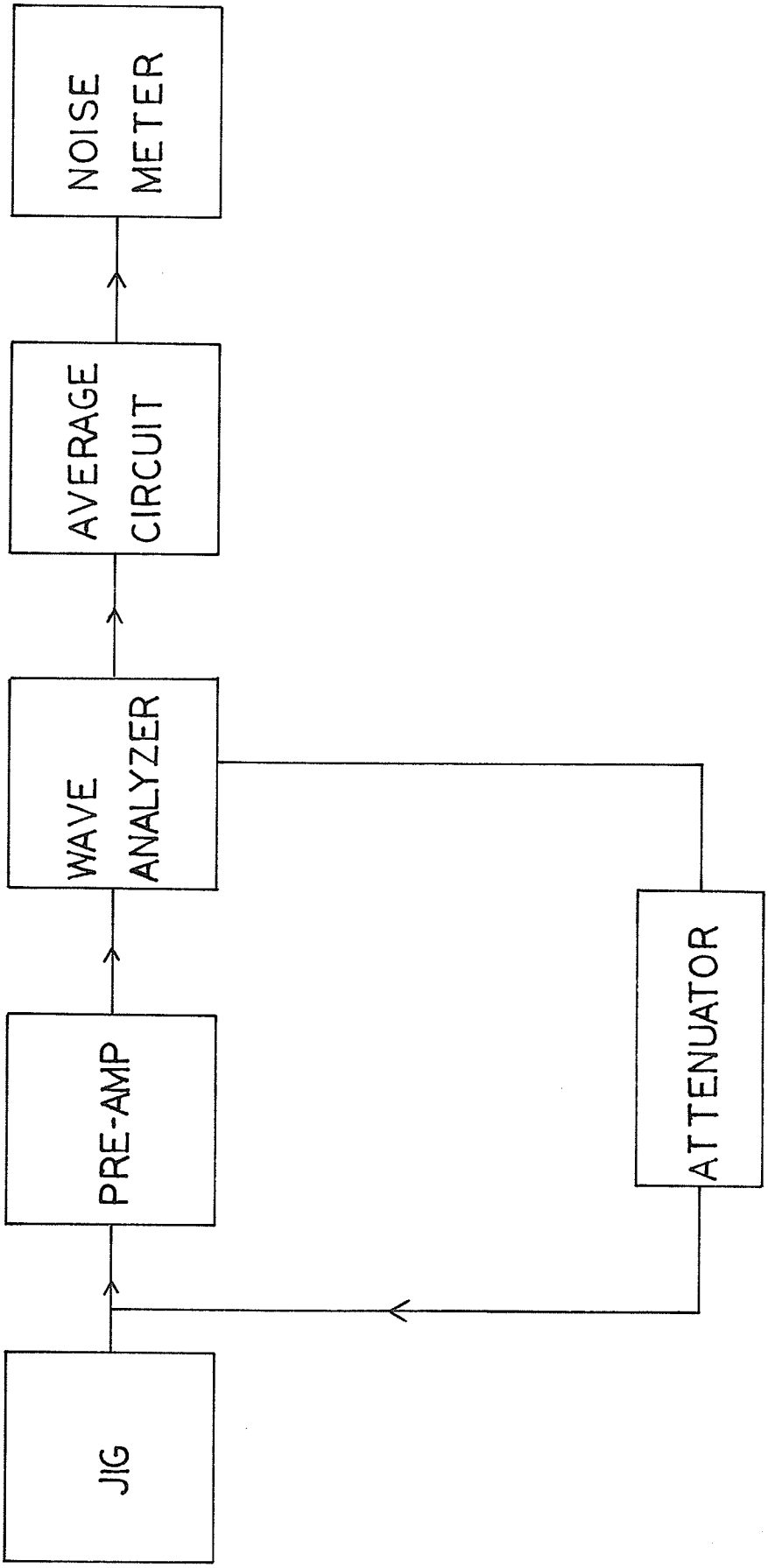

FIG. 4.3. BLOCK DIAGRAM REPRESENTATION (LOW FREQUENCY NOISE MEASUREMENT).

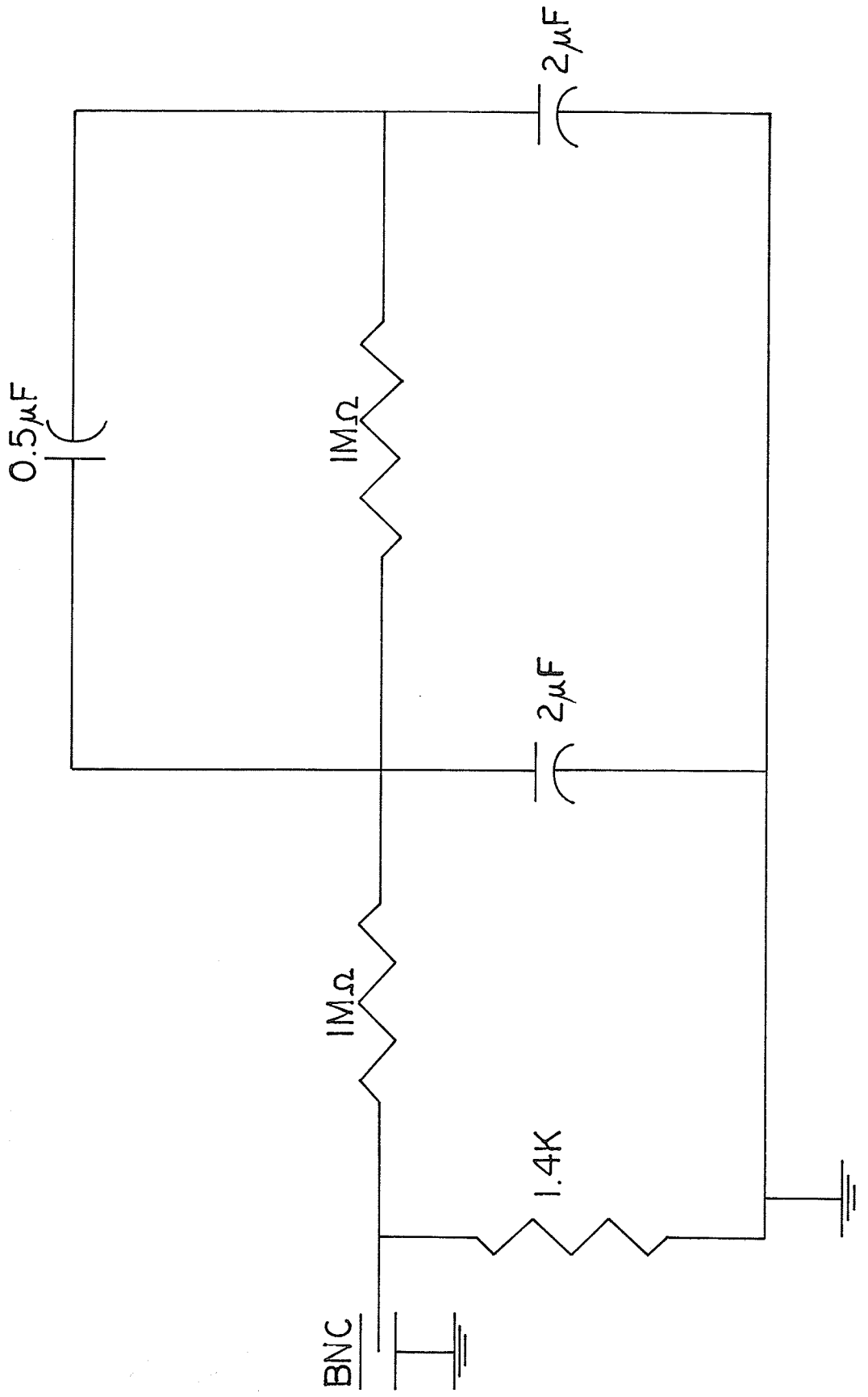

FIG. 4.4. AVERAGE CIRCUIT.

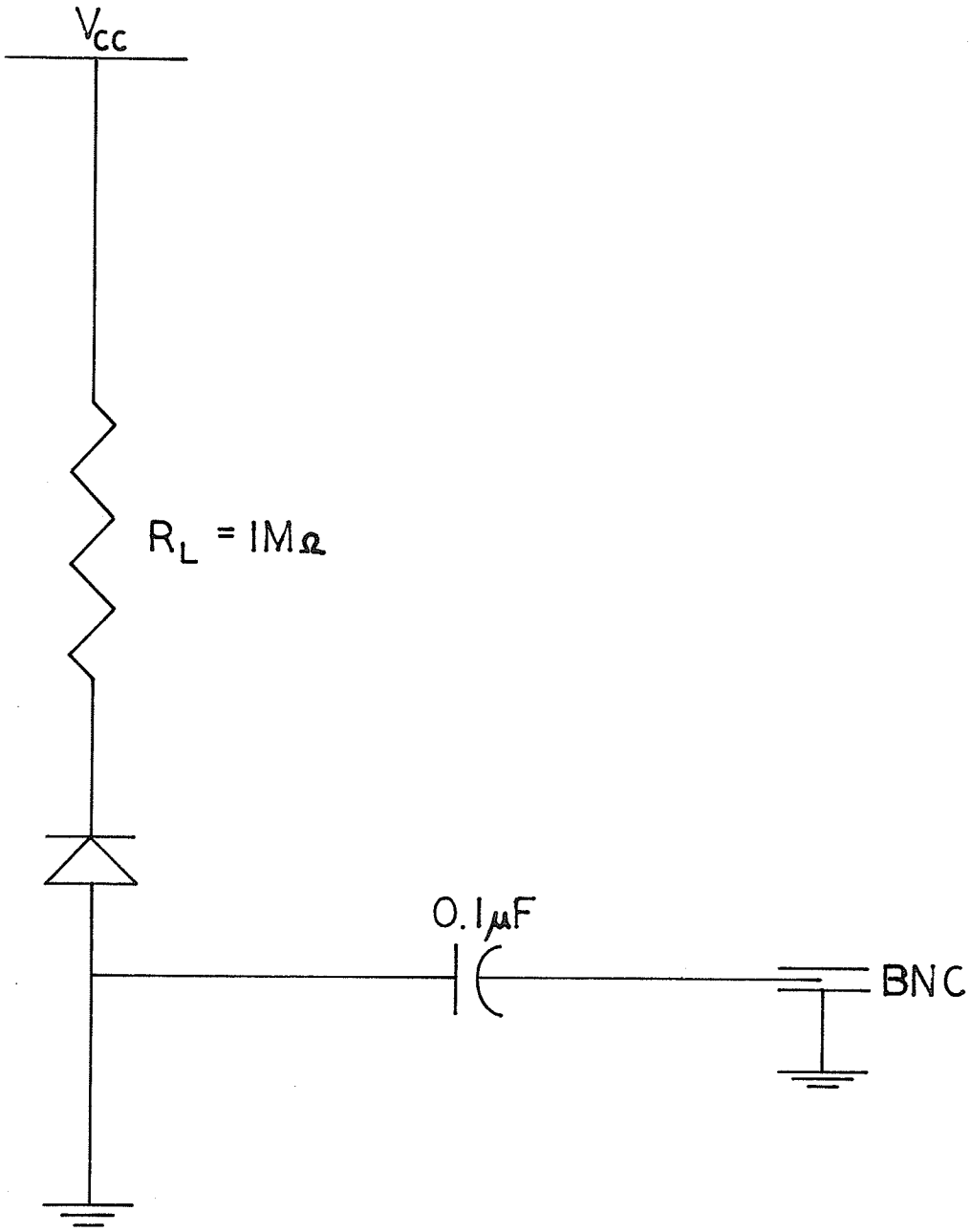

FIG. 4.5. JIG CIRCUIT.

Δf is the operating frequency of the oscilloscope

q = electronic charge = 1.6×10^{-19} coulombs

Δf = 6 c/s

$$\therefore \quad I_{eq} = \frac{\overline{i_o^2}}{2q\Delta f} = (\overline{i_o^2}) \times \frac{1}{6} \times \frac{1}{2q} \qquad \ldots(2)$$

with feedback through the attenuator

$$M_1 = K \sqrt{(\overline{i_o^2})}$$

where K is a constant

and M_1 is the noise meter reading when there is no input to the emitter.

If M_2 is the reading when feedback is connected

$$M_2 = K \sqrt{\overline{(i_o + \frac{V_{in}}{R})^2}}$$

$$= K \left[\overline{(i_o)^2 + (\frac{V_{in}}{R})^2 + 2\, i_o \frac{V_{in}}{R}} \right]^{1/2}$$

$\overline{i_o}$ is the average current

$$M_2 = K \left[(\overline{i_o})^2 + \overline{i_2} + 2\, \overline{i_o}\, \overline{i} \right]^{1/2}$$

$$= K \left[(\overline{i_o})^2 + \overline{i^2} \right]^{1/2}$$

where $i^2 = (\frac{V_{in}}{R})^2$ and $\overline{i} = o$,

$$\therefore \quad (M_1)^2 = K\, \overline{i_o^2}$$

$$(M_2)^2 = K\, (\overline{i_o^2} + \overline{i^2})$$

$$\therefore \quad \left(\frac{M_1}{M_2}\right)^2 = \frac{\overline{i_o^2}}{\overline{i_o}^2 + \overline{i^2}}$$

$$\overline{i^2} >> \overline{i_o}^2$$

$$\left(\frac{M_1}{M_2}\right)^2 \simeq \frac{\overline{i_o^2}}{\overline{i^2}}$$

$$\overline{i_o^2} = \frac{M_1}{M_2} \quad (\overline{i^2})$$

$$Ieq = \frac{1}{2q} \cdot (\overline{i^2}) \left(\frac{M_1}{M_2}\right)^2 \cdot \frac{1}{6}$$

$$= \frac{1}{12\ q} \left[\left(\frac{V_{in}}{R}\right)^2 \left(\frac{M_1}{M_2}\right)^2\right]$$

Biasing voltages were first turned on after the wave analyzer had been zero adjusted. A desired frequency was then set. At this frequency switch S (Figure 4.2) was opened and the reading appeared on the meter was recorded. This reading was referred to be M_1 according to theory. Then the switch S was closed and the necessary amount of attenuation was regulated. The reading indicated in the noise meter was M_2. Signal frequency was then varied and the whole measuring process was repeated. The range of frequency used were from 20 hz to 45 khz. The results were used to calculate Ieq as stated in the theory and Ieq vs frequency was plotted, (Figure 5.1). The

DC current flow was also recorded and graphs of I_{DC} vs Ieq and I verses V were plotted as shown in Figure 5.2 and Figure 5.3, respectively.

4.2.3 Photoconductivity Test

A pulsed light source was connected to the circuit shown in Figure 4.6. The circuit of the operational amplifier is shown in Figure 4.7. The gain of the amplifying circuit was 300. Light pulses were shone on the sample which was biased near its breakdown voltage and the response characteristics were observed on the oscilloscope. Figure 5.11 showed the shape of the output response. Pulse frequency as well as light intensity were varied in order to check whether there were any change in the shape of the response.

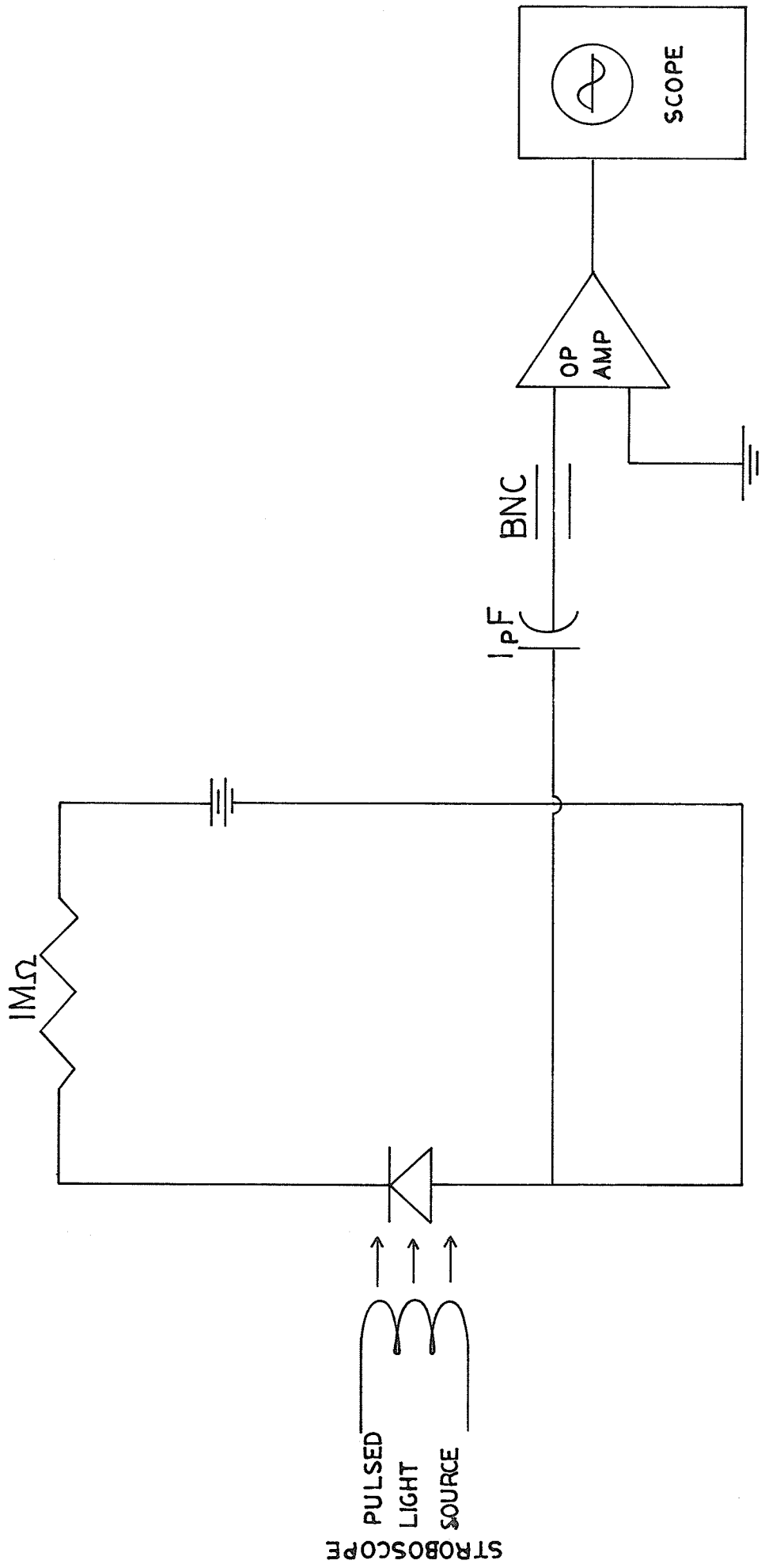

FIG. 4.6. PHOTOCONDUCTIVITY MEASUREMENT.

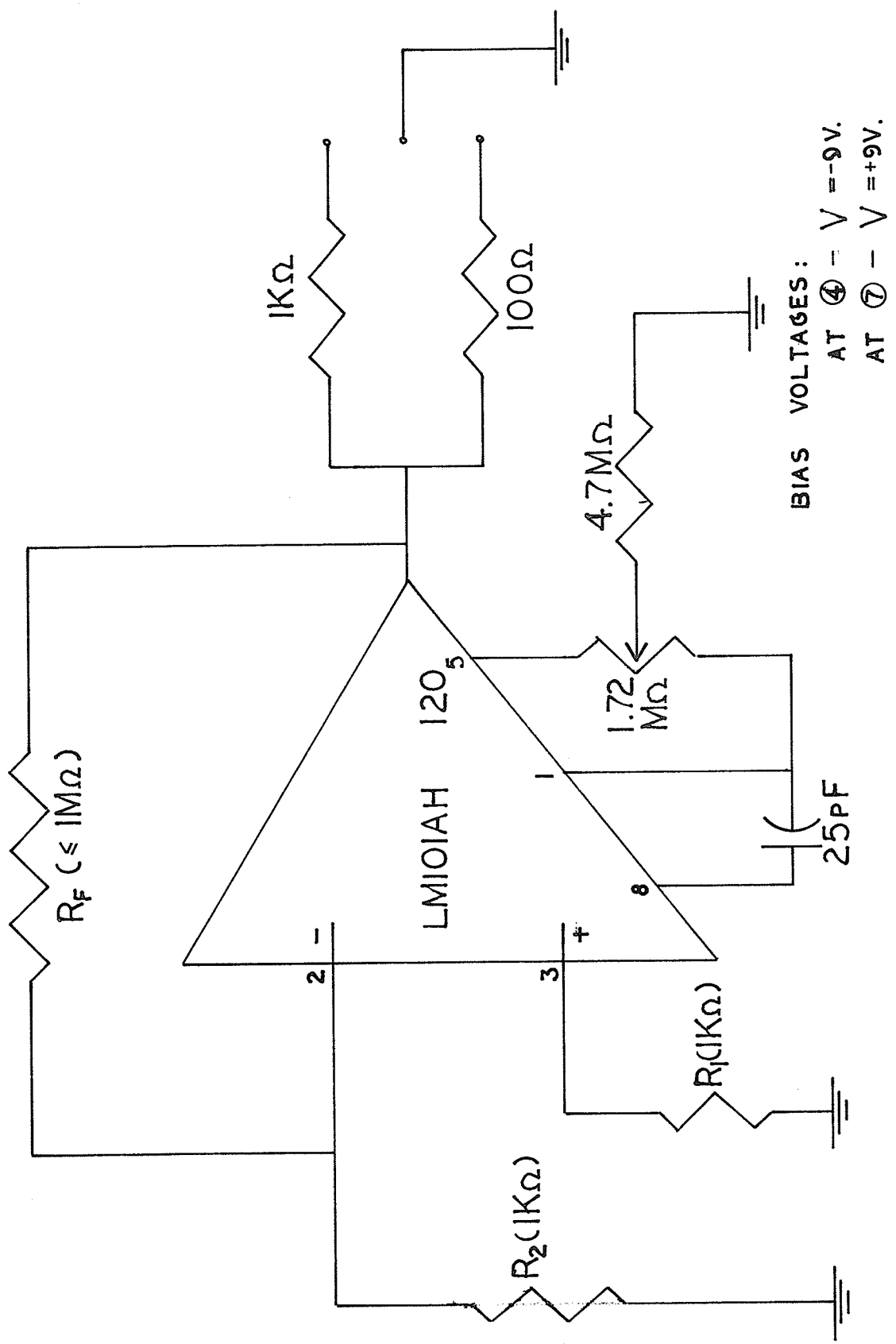

FIG. 4.7. OPERATIONAL AMPLIFIER CONNECTIONS.

CHAPTER V

EXPERIMENTAL RESULTS AND DATA

In this chapter the results of experiments discussed in Chapter IV are presented. Figures 5.1 and 5.2 are results from the noise measurement experiment. Figure 5.3 is the V-I characteristic of the anthracene sample measured up to its breakdown value. Figures 5.4, 5.5 and 5.6 are experimental results obtained by Hsu for silicon temperature coefficients.

The temperature coefficient of anthracene is presented in Figure 5.7 and it is compared with the measured data for silicon. With the aid of computer, the range of the circuit elements in the proposed microplasma model is determined. The characteristic admittances of the assumed model during turn-on and turn-off of the microplasma model are then calculated and the computer plots for the same are presented in Figures 5.9 and 5.10.

Pictures on microplasma and photoconductivity of anthracene under high field are shown in Figures 5.11, 5.12 and 5.13, respectively.

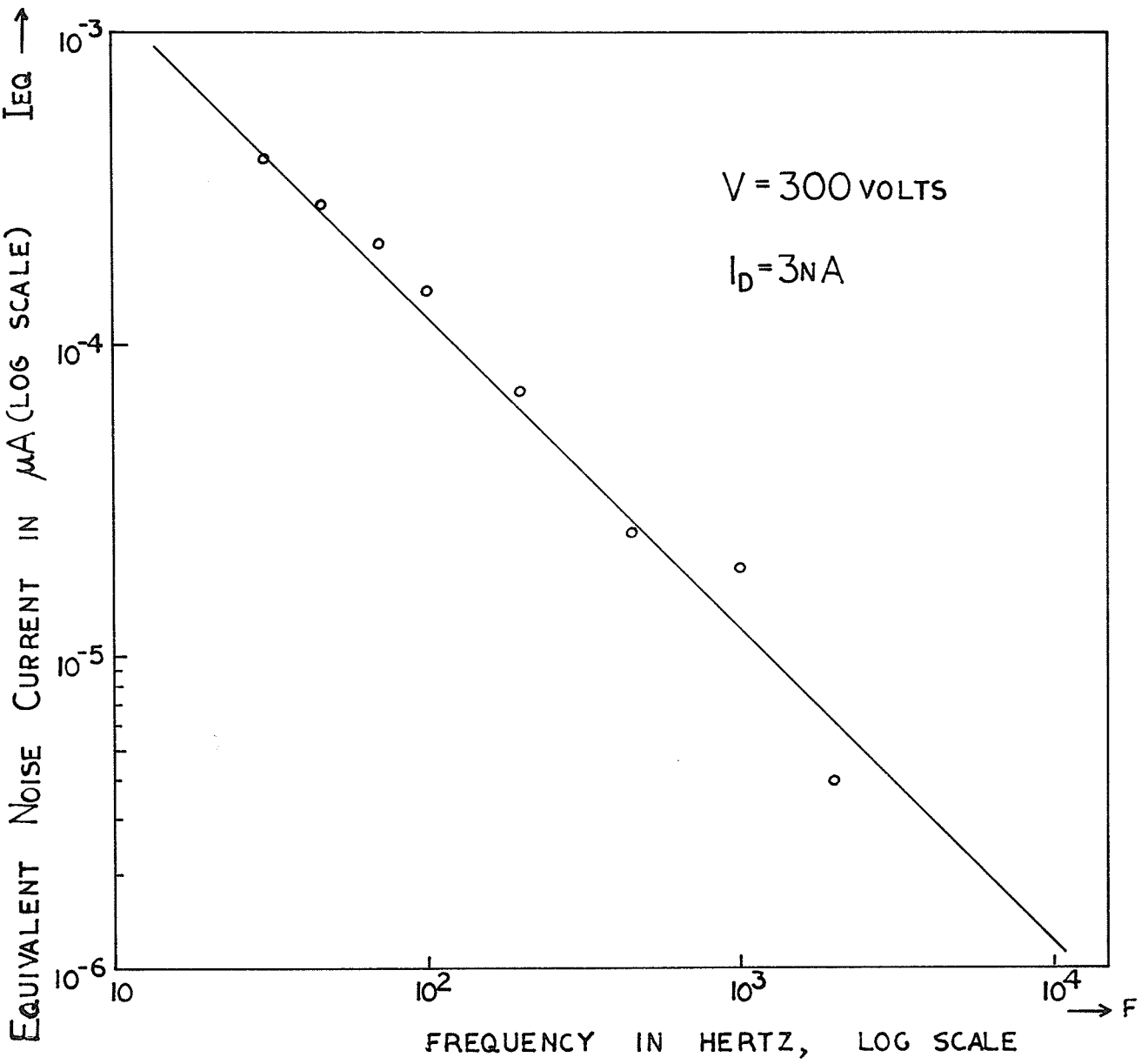

FIG. 5.1. GRAPH OF NOISE EQUIVALENT CURRENT VS FREQUENCY.

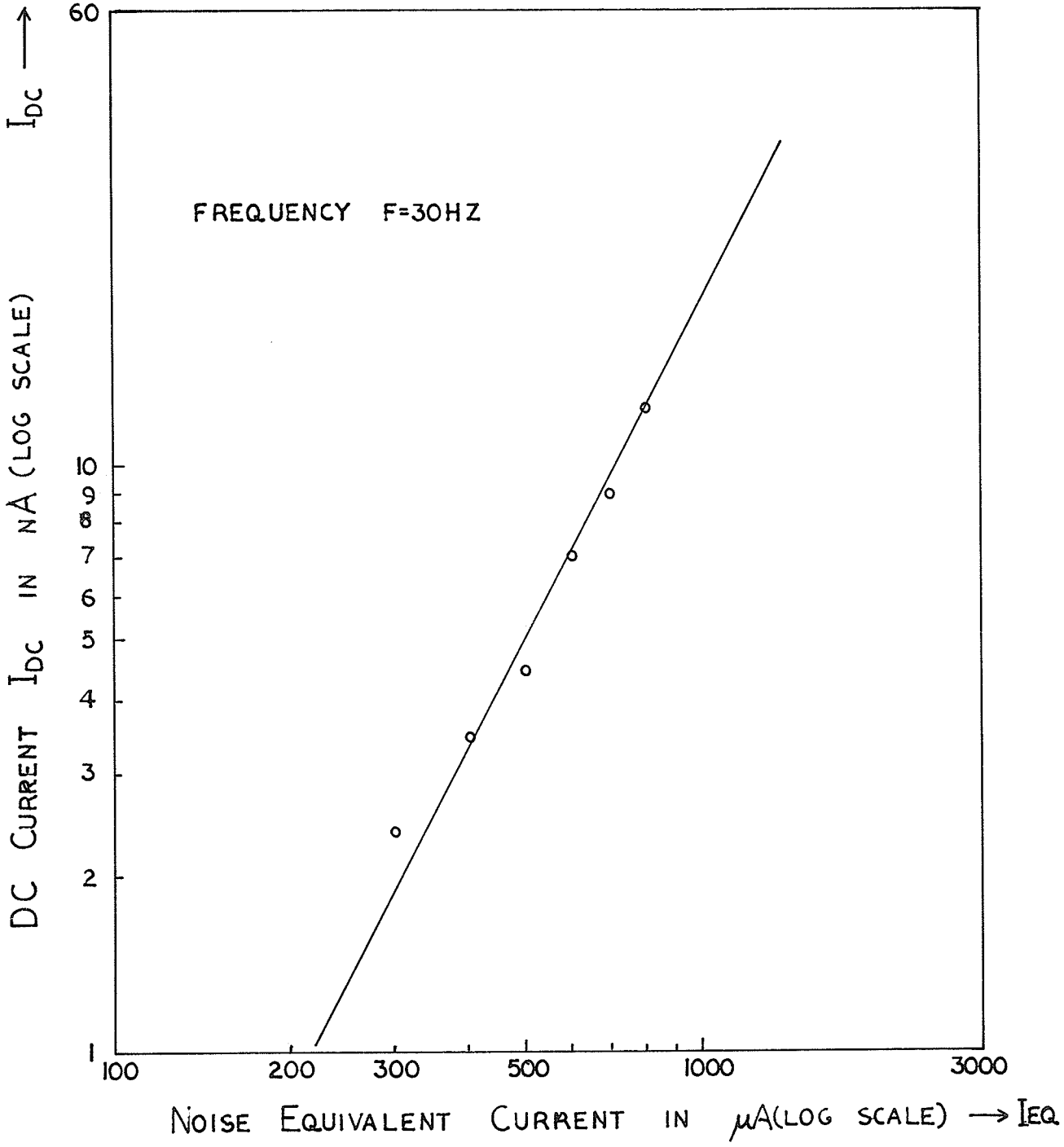

FIG. 5.2. GRAPH OF DC CURRENT VS NOISE EQUIVALENT CURRENT.

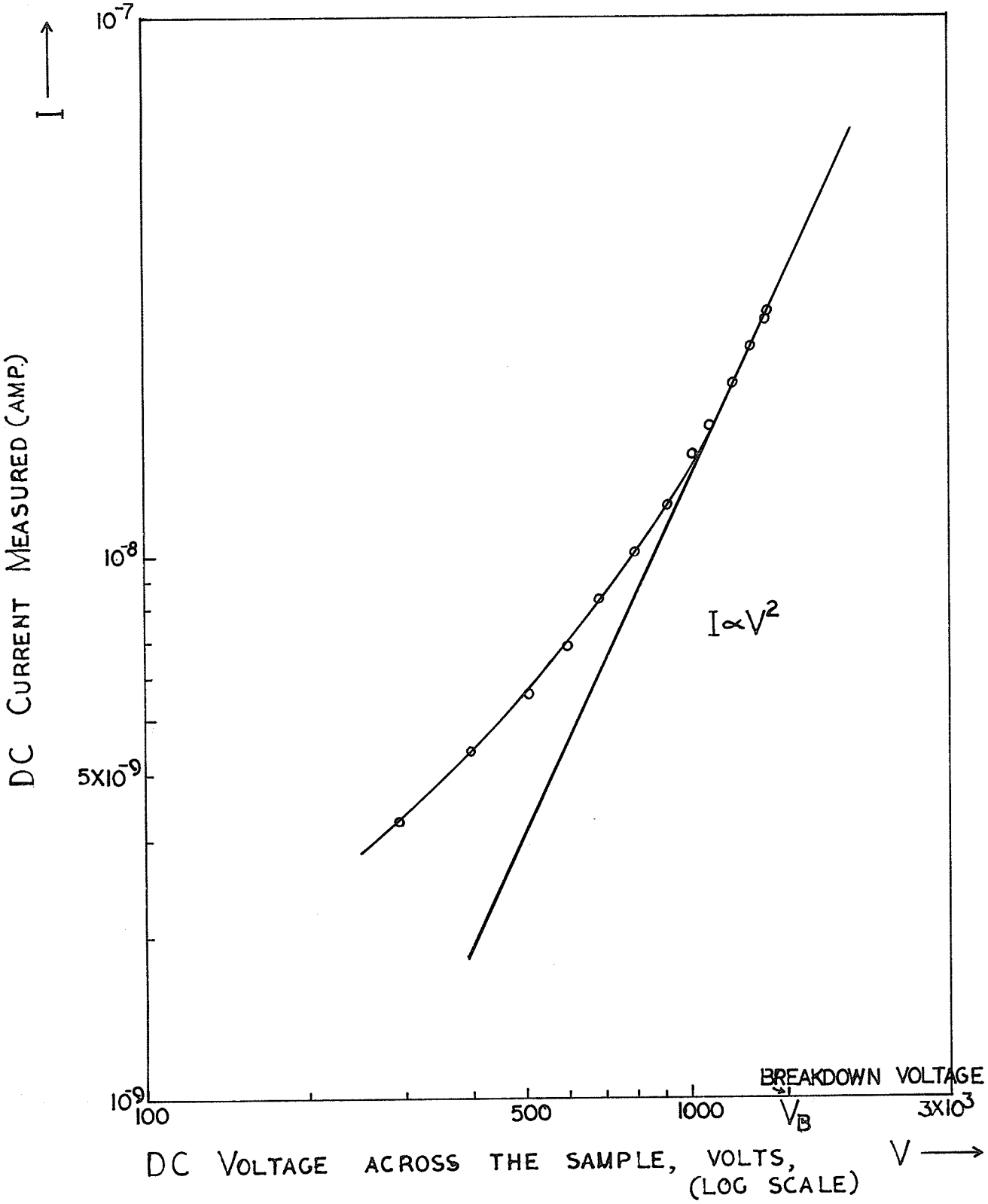

FIG. 5.3. GRAPH OF DC CHARACTERISTIC OF THE SAMPLE.

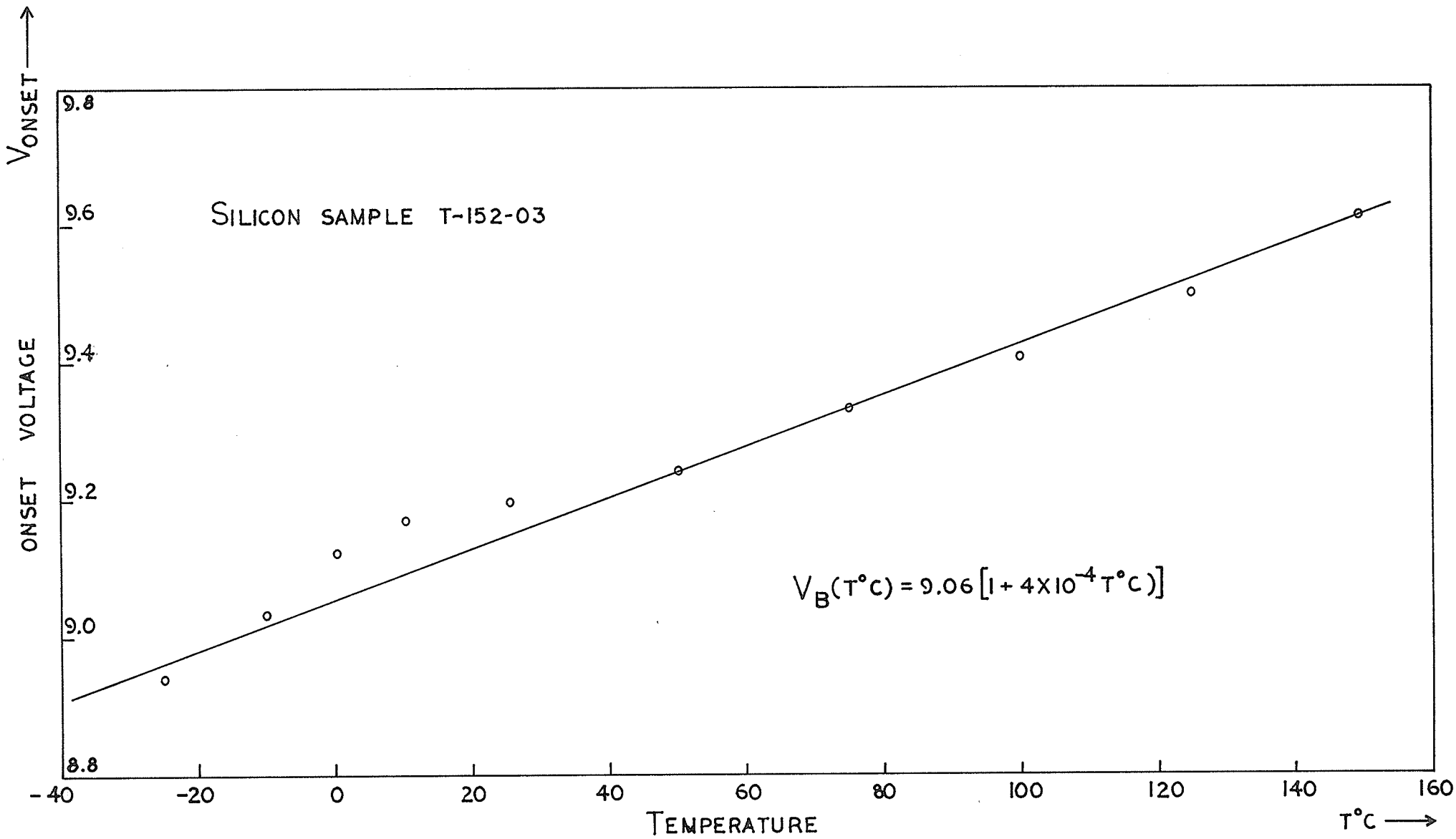

FIG. 5.4. ONSET OF MICROPLASMA NOISE VS TEMPERATURE.

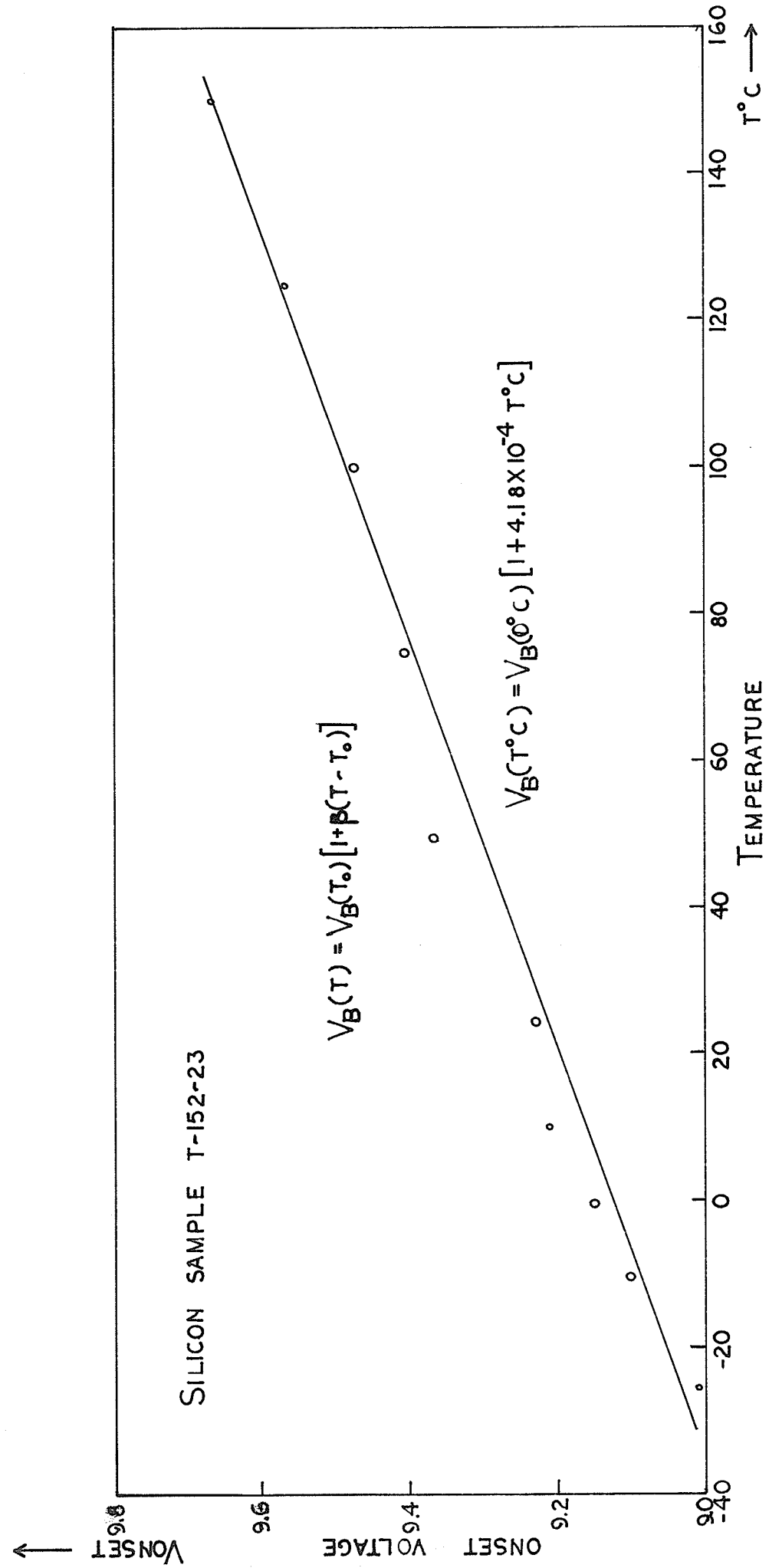

FIG. 5.5. MICROPLASMA ONSET VOLTAGE VS TEMPERATURE.

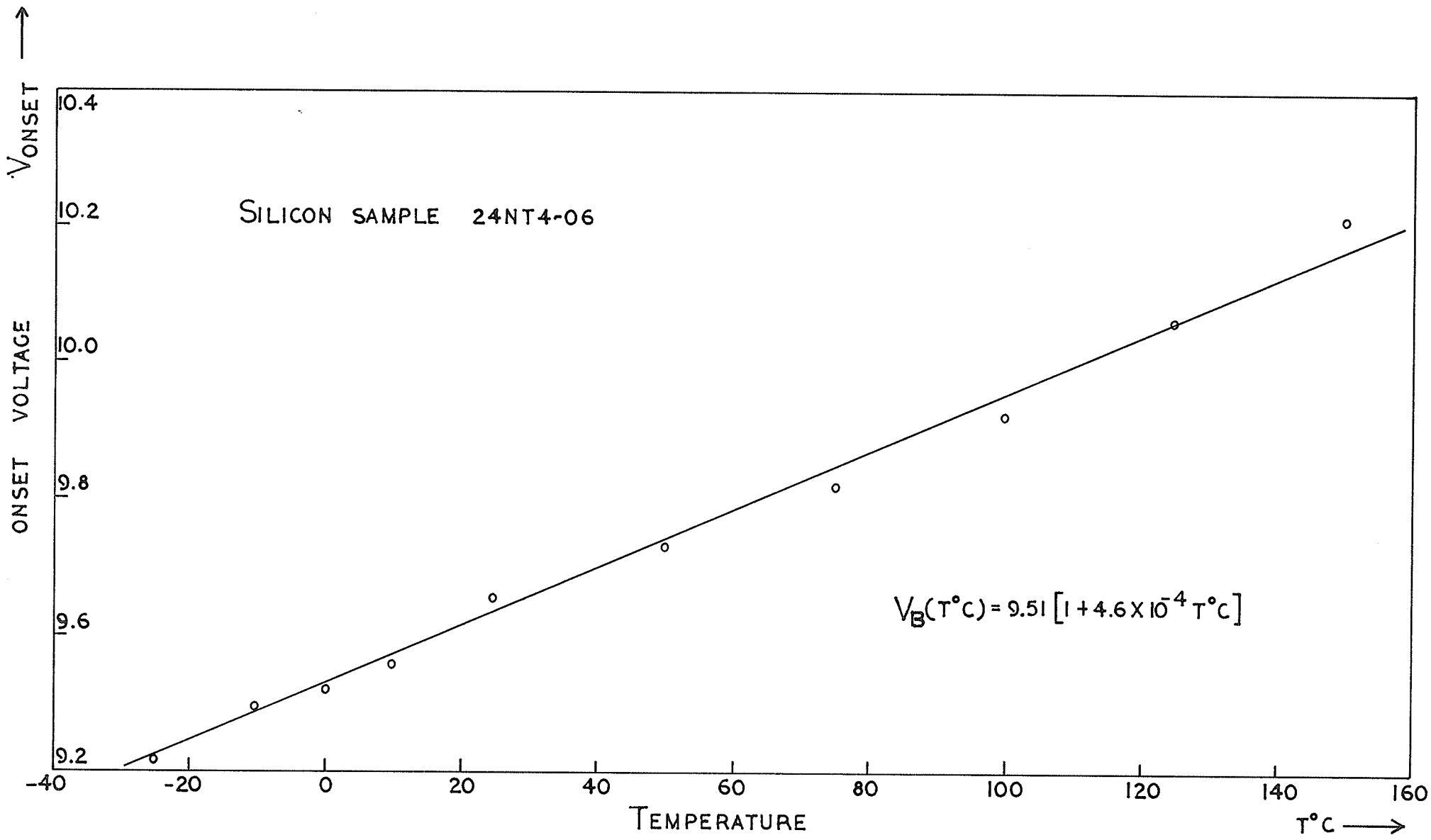

FIG. 5.6. ONSET OF MICROPLASMA NOISE VS TEMPERATURE.

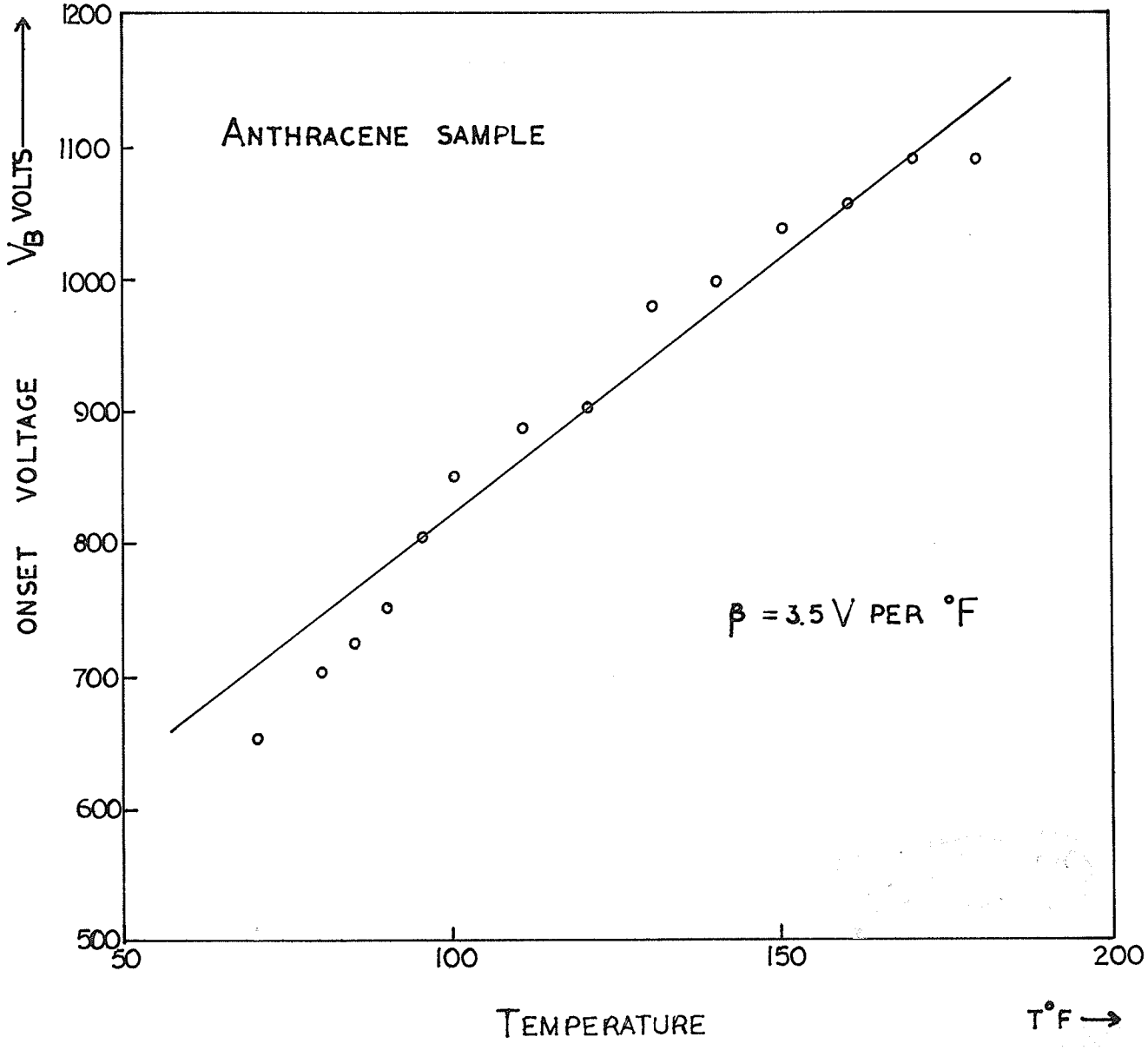

FIG. 5.7. ONSET OF MICROPLASMA VS TEMPERATURE.

The theoretical model of microplasma was analyzed by computer. The results were tabulated as follows:

Step-Size for Computing	R_1	R	R_2	C_1	C_2	Time Constants	
						τ_1	τ_2
(μ sec)	(MΩ)	(MΩ)	(MΩ)	(pf)	(pf)	(μ sec)	(μ sec)
1.0	0.1	10	0.01	0.01	1.0	10.00	0.9182
1.0	1.0	10	1.0	0.01	1.0	9.258	5.05
1.0	0.1	10	0.1	0.01	1.0	10.0	5.05
0.1	0.1	10	0.01	0.01	0.1	1.089	0.1
0.1	0.01	10	0.01	0.001	0.1	0.1	0.0505

τ_1 is the time constant for the turn-off case.

τ_2 is the time constant for the turn-on case.

Computer plots for admittances during turn-on and turn-off of microplasma were made for each set of values. Comparison with pictures for current fluctuation during microplasma breakdown by Champlin [5] was made. The curves that were closely similar in shape to Champlin's results were chosen. The element values of the model corresponding to the chosen curves were presented in Figure 5.8.

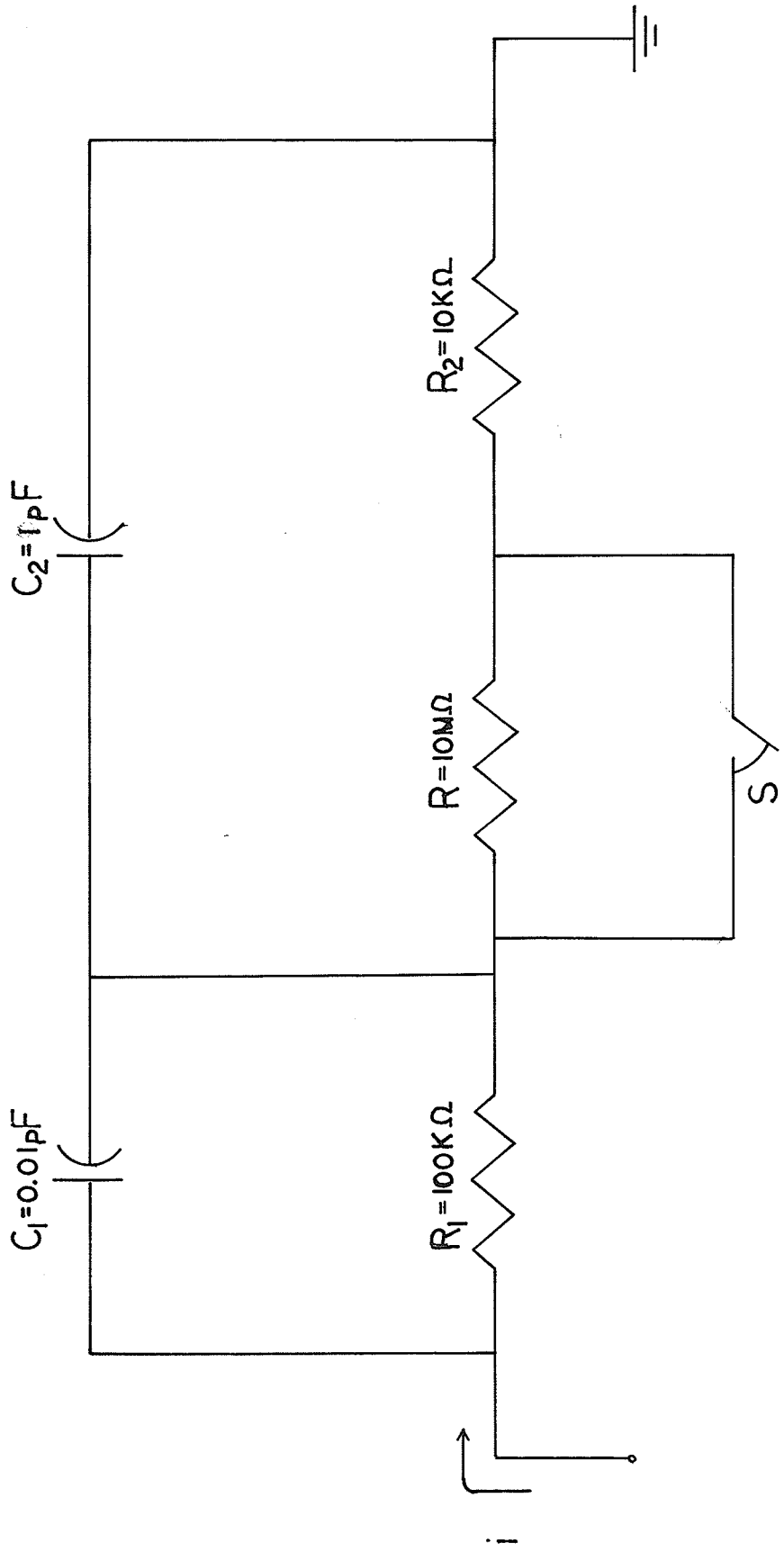

FIG. 5.8. MICROPLASMA MODEL WITH APPROXIMATED ELEMENT VALUES.

DIODE TURN-ON TIME CONSTANT = 0.9182E-06

TIME (SEC.)	ADMITTANCE VALUES	
	G1(MHOS)	G2(MHOS)
0.0	0.900099E-05	0.909003E-05
0.000001	0.815395E-05	0.909061E-05
0.000002	0.738733E-05	0.909081E-05
0.000003	0.669375E-05	0.909088E-05
0.000004	0.606618E-05	0.909090E-05
0.000005	0.549832E-05	0.909090E-05
0.000006	0.498450E-05	0.909091E-05
0.000007	0.451958E-05	0.909091E-05
0.000008	0.409890E-05	0.909091E-05
0.000009	0.371826E-05	0.909091E-05
0.000010	0.337383E-05	0.909091E-05
0.000011	0.306219E-05	0.909091E-05
0.000012	0.278020E-05	0.909091E-05
0.000013	0.252504E-05	0.909091E-05
0.000014	0.229417E-05	0.909091E-05
0.000015	0.208526E-05	0.909091E-05
0.000016	0.189624E-05	0.909091E-05
0.000017	0.172520E-05	0.909091E-05
0.000018	0.157044E-05	0.909091E-05
0.000019	0.143041E-05	0.909091E-05
0.000020	0.130370E-05	0.909091E-05
0.000021	0.118905E-05	0.909091E-05
0.000022	0.108531E-05	0.909091E-05
0.000023	0.991444E-06	0.909091E-05
0.000024	0.906510E-06	0.909091E-05
0.000025	0.829658E-06	0.909091E-05
0.000026	0.760118E-06	0.909091E-05
0.000027	0.697197E-06	0.909091E-05
0.000028	0.640263E-06	0.909091E-05
0.000029	0.588747E-06	0.909091E-05
0.000030	0.542133E-06	0.909091E-05
0.000031	0.499956E-06	0.909091E-05
0.000032	0.461791E-06	0.909091E-05
0.000033	0.427259E-06	0.909091E-05
0.000034	0.396013E-06	0.909091E-05
0.000035	0.367741E-06	0.909091E-05
0.000036	0.342158E-06	0.909091E-05
0.000037	0.319010E-06	0.909091E-05
0.000038	0.298066E-06	0.909091E-05
0.000039	0.279114E-06	0.909091E-05
0.000040	0.261966E-06	0.909091E-05
0.000041	0.246449E-06	0.909091E-05
0.000042	0.232403E-06	0.909091E-05
0.000043	0.219705E-06	0.909091E-05
0.000044	0.208210E-06	0.909091E-05
0.000045	0.197809E-06	0.909091E-05
0.000046	0.188398E-06	0.909091E-05
0.000047	0.179882E-06	0.909091E-05
0.000048	0.172177E-06	0.909091E-05
0.000049	0.165205E-06	0.909091E-05
0.000050	0.158897E-06	0.909091E-05
0.000051	0.153188E-06	0.909091E-05
0.000052	0.148023E-06	0.909091E-05
0.000053	0.143350E-06	0.909091E-05
0.000054	0.139121E-06	0.909091E-05
0.000055	0.135295E-06	0.909091E-05
0.000056	0.131832E-06	0.909091E-05
0.000057	0.128700E-06	0.909091E-05

0.000060	0.123979E-06	0.909091E-05
0.000061	0.118879E-06	0.909091E-05
0.000062	0.116979E-06	0.909091E-05
0.000063	0.115260E-06	0.909091E-05
0.000064	0.113704E-06	0.909091E-05
0.000065	0.112296E-06	0.909091E-05
0.000066	0.111023E-06	0.909091E-05
0.000067	0.109870E-06	0.909091E-05
0.000068	0.108827E-06	0.909091E-05
0.000069	0.107884E-06	0.909091E-05
0.000070	0.107030E-06	0.909091E-05
0.000071	0.106258E-06	0.909091E-05
0.000072	0.105558E-06	0.909091E-05
0.000073	0.104926E-06	0.909091E-05
0.000074	0.104354E-06	0.909091E-05
0.000075	0.103836E-06	0.909091E-05
0.000076	0.103367E-06	0.909091E-05
0.000077	0.102943E-06	0.909091E-05
0.000078	0.102560E-06	0.909091E-05
0.000079	0.102212E-06	0.909091E-05
0.000080	0.101898E-06	0.909091E-05
0.000081	0.101614E-06	0.909091E-05
0.000082	0.101357E-06	0.909091E-05
0.000083	0.101124E-06	0.909091E-05
0.000084	0.100914E-06	0.909091E-05
0.000085	0.100723E-06	0.909091E-05
0.000086	0.100551E-06	0.909091E-05
0.000087	0.100395E-06	0.909091E-05
0.000088	0.100254E-06	0.909091E-05
0.000089	0.100126E-06	0.909091E-05
0.000090	0.100011E-06	0.909091E-05
0.000091	0.999060E-07	0.909091E-05
0.000092	0.998114E-07	0.909091E-05
0.000093	0.997259E-07	0.909091E-05
0.000094	0.996484E-07	0.909091E-05
0.000095	0.995782E-07	0.909091E-05
0.000096	0.995149E-07	0.909091E-05
0.000097	0.994575E-07	0.909091E-05
0.000098	0.994056E-07	0.909091E-05
0.000099	0.993585E-07	0.909091E-05
0.000100	0.993161E-07	0.909091E-05
0.000101	0.992776E-07	0.909091E-05
0.000102	0.992428E-07	0.909091E-05
0.000103	0.992113E-07	0.909091E-05
0.000104	0.991828E-07	0.909091E-05
0.000105	0.991570E-07	0.909091E-05
0.000106	0.991337E-07	0.909091E-05
0.000107	0.991126E-07	0.909091E-05
0.000108	0.990935E-07	0.909091E-05
0.000109	0.990762E-07	0.909091E-05
0.000110	0.990605E-07	0.909091E-05
0.000111	0.990464E-07	0.909091E-05
0.000112	0.990336E-07	0.909091E-05
0.000113	0.990220E-07	0.909091E-05
0.000114	0.990115E-07	0.909091E-05
0.000115	0.990021E-07	0.909091E-05
0.000116	0.989935E-07	0.909091E-05
0.000117	0.989857E-07	0.909091E-05
0.000118	0.989787E-07	0.909091E-05
0.000119	0.989724E-07	0.909091E-05
0.000120	0.989666E-07	0.909091E-05
0.000121	0.989614E-07	0.909091E-05
0.000122	0.989567E-07	0.909091E-05
0.000123	0.989524E-07	

0.000124	0.989485E-07	0.909091E-05
0.000125	0.989451E-07	0.909091E-05
0.000126	0.989419E-07	0.909091E-05
0.000127	0.989390E-07	0.909091E-05
0.000128	0.989365E-07	0.909091E-05
0.000129	0.989341E-07	0.909091E-05
0.000130	0.989320E-07	0.909091E-05
0.000131	0.989301E-07	0.909091E-05
0.000132	0.989284E-07	0.909091E-05
0.000133	0.989268E-07	0.909091E-05
0.000134	0.989253E-07	0.909091E-05
0.000135	0.989241E-07	0.909091E-05
0.000136	0.989229E-07	0.909091E-05
0.000137	0.989219E-07	0.909091E-05
0.000138	0.989209E-07	0.909091E-05
0.000139	0.989201E-07	0.909091E-05
0.000140	0.989193E-07	0.909091E-05
0.000141	0.989186E-07	0.909091E-05
0.000142	0.989179E-07	0.909091E-05
0.000143	0.989173E-07	0.909091E-05
0.000144	0.989169E-07	0.909091E-05
0.000145	0.989164E-07	0.909091E-05
0.000146	0.989160E-07	0.909091E-05
0.000147	0.989156E-07	0.909091E-05
0.000148	0.989152E-07	0.909091E-05
0.000149	0.989149E-07	0.909091E-05
0.000150	0.989146E-07	0.909091E-05
0.000151	0.989143E-07	0.909091E-05
0.000152	0.989141E-07	0.909091E-05
0.000153	0.989139E-07	0.909091E-05
0.000154	0.989137E-07	0.909091E-05
0.000155	0.989135E-07	0.909091E-05
0.000156	0.989133E-07	0.909091E-05
0.000157	0.989132E-07	0.909091E-05
0.000158	0.989131E-07	0.909091E-05
0.000159	0.989129E-07	0.909091E-05
0.000160	0.989128E-07	0.909091E-05
0.000161	0.989128E-07	0.909091E-05
0.000162	0.989127E-07	0.909091E-05
0.000163	0.989126E-07	0.909091E-05
0.000164	0.989125E-07	0.909091E-05
0.000165	0.989124E-07	0.909091E-05

0.000170	0.989123E-07	0.909091E-05
0.000171	0.989122E-07	0.909091E-05
0.000172	0.989122E-07	0.909091E-05
0.000173	0.989122E-07	0.909091E-05
0.000174	0.989122E-07	0.909091E-05
0.000175	0.989121E-07	0.909091E-05
0.000176	0.989121E-07	0.909091E-05
0.000177	0.989121E-07	0.909091E-05
0.000178	0.989120E-07	0.909091E-05
0.000179	0.989120E-07	0.909091E-05
0.000180	0.989120E-07	0.909091E-05
0.000181	0.989120E-07	0.909091E-05
0.000182	0.989120E-07	0.909091E-05
0.000183	0.989120E-07	0.909091E-05
0.000184	0.989120E-07	0.909091E-05
0.000185	0.989120E-07	0.909091E-05
0.000186	0.989120E-07	0.909091E-05
0.000187	0.989120E-07	0.909091E-05
0.000188	0.989120E-07	0.909091E-05
0.000189	0.989119E-07	0.909091E-05
0.000190	0.989119E-07	0.909091E-05
0.000191	0.989119E-07	0.909091E-05
0.000192	0.989119E-07	0.909091E-05
0.000193	0.989119E-07	0.909091E-05
0.000194	0.989119E-07	0.909091E-05
0.000195	0.989119E-07	0.909091E-05
0.000196	0.989119E-07	0.909091E-05
0.000197	0.989119E-07	0.909091E-05
0.000198	0.989119E-07	0.909091E-05
0.000199	0.989119E-07	0.909091E-05
0.000200	0.989119E-07	0.909091E-05
0.000201	0.989119E-07	0.909091E-05
0.000202	0.989119E-07	0.909091E-05
0.000203	0.989119E-07	0.909091E-05
0.000204	0.989119E-07	0.909091E-05
0.000205	0.989119E-07	0.909091E-05
0.000206	0.989119E-07	0.909091E-05

0.000208	0.989119E-07	0.909091E-05
0.000209	0.989119E-07	0.909091E-05
0.000210	0.989119E-07	0.909091E-05
0.000211	0.989119E-07	0.909091E-05
0.000212	0.989119E-07	0.909091E-05
0.000213	0.989119E-07	0.909091E-05
0.000214	0.989119E-07	0.909091E-05
0.000215	0.989119E-07	0.909091E-05
0.000216	0.989119E-07	0.909091E-05
0.000217	0.989119E-07	0.909091E-05
0.000218	0.989119E-07	0.909091E-05
0.000219	0.989119E-07	0.909091E-05
0.000220	0.989119E-07	0.909091E-05
0.000221	0.989119E-07	0.909091E-05
0.000222	0.989119E-07	0.909091E-05
0.000223	0.989119E-07	0.909091E-05
0.000224	0.989119E-07	0.909091E-05
0.000225	0.989119E-07	0.909091E-05
0.000226	0.989119E-07	0.909091E-05
0.000227	0.989119E-07	0.909091E-05
0.000228	0.989119E-07	0.909091E-05
0.000229	0.989119E-07	0.909091E-05
0.000230	0.989119E-07	0.909091E-05
0.000231	0.989119E-07	0.909091E-05
0.000232	0.989119E-07	0.909091E-05
0.000233	0.989119E-07	0.909091E-05
0.000234	0.989119E-07	0.909091E-05
0.000235	0.989119E-07	0.909091E-05
0.000236	0.989119E-07	0.909091E-05
0.000237	0.989119E-07	0.909091E-05
0.000238	0.989119E-07	0.909091E-05
0.000239	0.989119E-07	0.909091E-05
0.000240	0.989119E-07	0.909091E-05
0.000241	0.989119E-07	0.909091E-05
0.000242	0.989119E-07	0.909091E-05
0.000243	0.989119E-07	0.909091E-05
0.000244	0.989119E-07	0.909091E-05
0.000245	0.989119E-07	0.909091E-05
0.000246	0.989119E-07	0.909091E-05
0.000247	0.989119E-07	0.909091E-05
0.000248	0.989119E-07	0.909091E-05
0.000249	0.989119E-07	0.909091E-05
0.000250	0.989119E-07	0.909091E-05
0.000251	0.989119E-07	0.909091E-05
0.000252	0.989119E-07	0.909091E-05
0.000253	0.989119E-07	0.909091E-05
0.000254	0.989119E-07	0.909091E-05
0.000255	0.989119E-07	0.909091E-05
0.000256	0.989119E-07	0.909091E-05
0.000257	0.989119E-07	0.909091E-05
0.000258	0.989119E-07	0.909091E-05
0.000259	0.989119E-07	0.909091E-05

FIGURE 5.9

THEORETICAL ADMITTANCE CHARACTERISTIC OF MICROPLASMA I
ANTHRACENE DIODE AFTER TURN-OFF

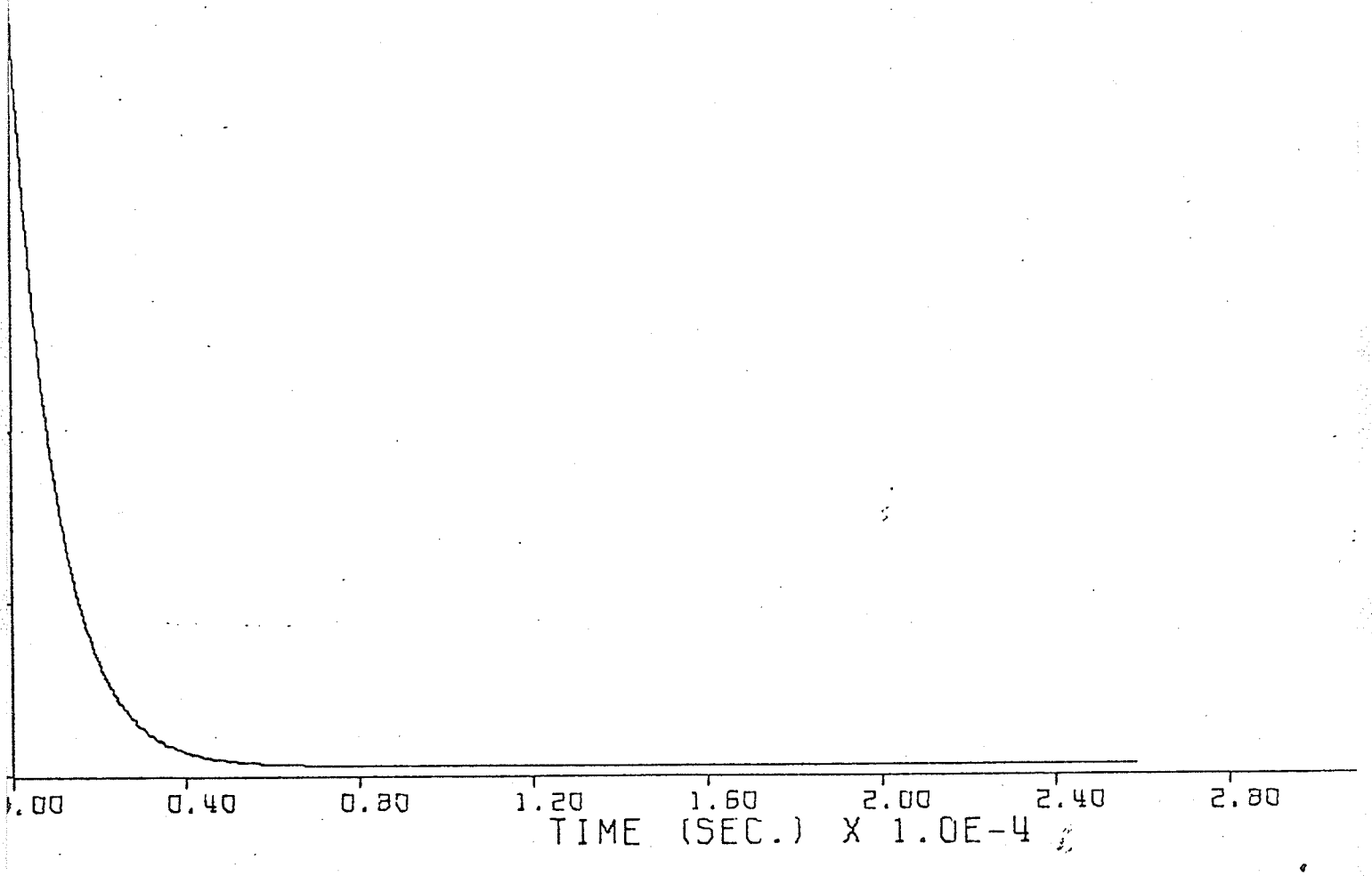

FIGURE 5.10

THEORETICAL ADMITTANCE CHARACTERISTIC OF MICROPLASMA I
ANTHRACENE DIODE AFTER TURN-ON

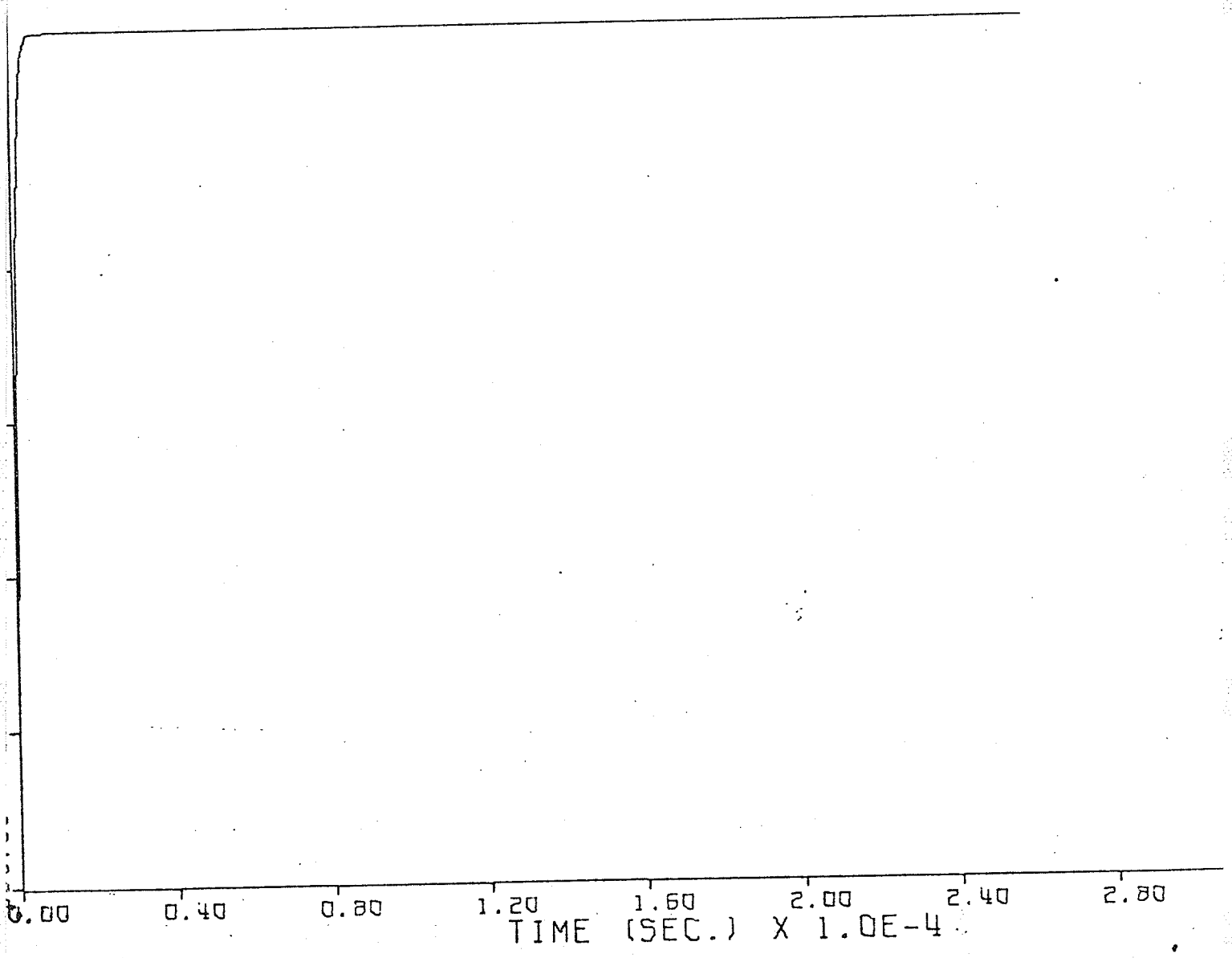

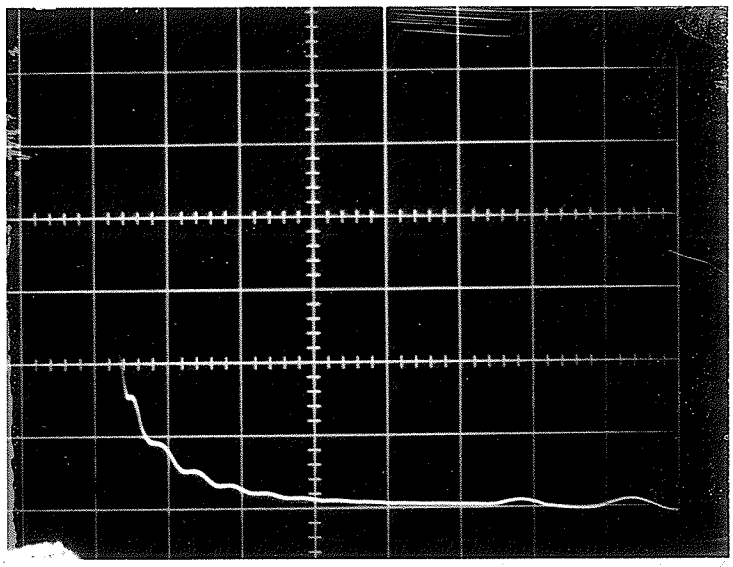

FIG. 5.11 SHAPE OF OUTPUT RESPONSE IN PHOTOCONDUCTIVITY TEST

Sweep Rate = 20 μsec

Voltage Scale = 0.1 v. /div.

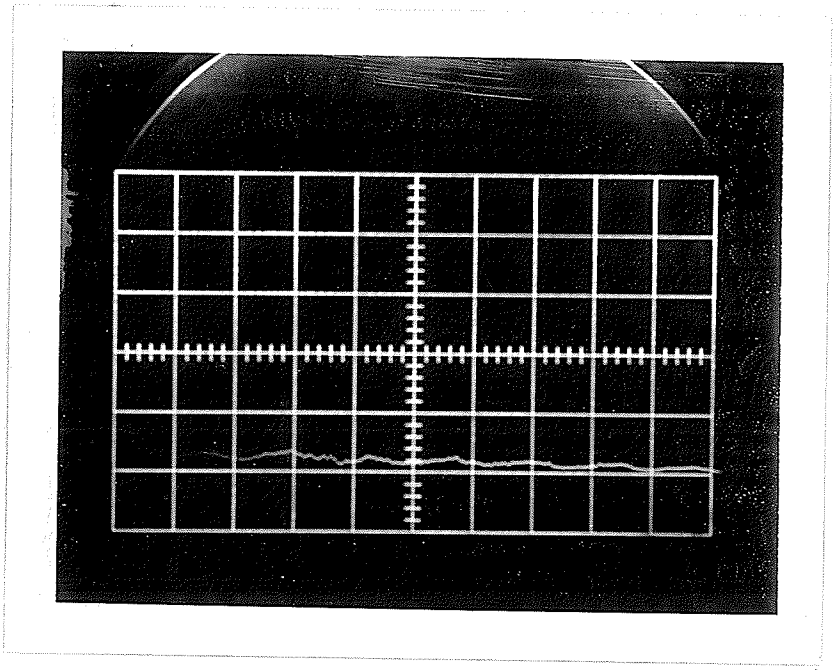

FIG. 5.12

MICROPLASMA BREAKDOWN IN ANTHRACENE HOLE-INJECTION DIODE

Sweep Time = 50 μsec.; Voltage Scale = 0.2 v./div.

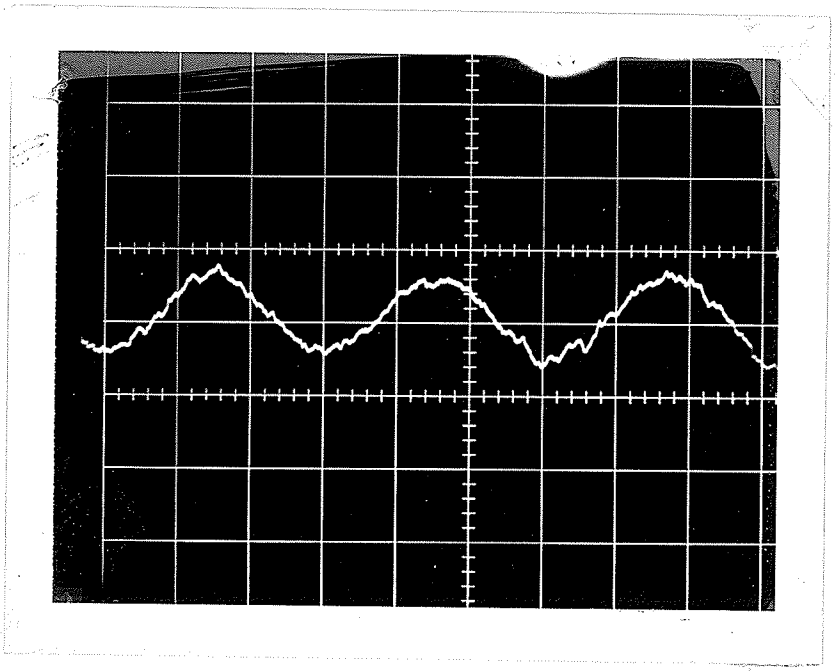

FIG. 5.13

MICROPLASMA BREAKDOWN IN ANTHRACENE HOLE-INJECTION DIODE

Sweep Time = 5 msec.; Voltage Scale = 2 mv/div.

CHAPTER VI

ANALYSIS OF EXPERIMENTAL RESULTS AND DISCUSSIONS

Low frequency noise of space-charge-limited diodes made of single anthracene crystal has been studied. The low frequency noise spectrum, the low frequency noise power as a function of DC bias voltage as well as the DC current-voltage characteristic have been measured.

From the current-voltage plot, it was observed that the slope of graph was 2 at higher voltages. The current is thus proportional to the square of voltages. This observation led us to suggest that the voltage region was in the space-charge-limited region. This is justified by the space-charge-limited current equation, (Child-Langmuir's Law), that

$$I \simeq 10^{-13} V^2 \mu\varepsilon/d^3 \quad \text{amp-cm}^{-2} \qquad \ldots(1)$$

At that voltage, the concentration of free carriers injected from the contact becomes considerably greater than the concentrating of majority carriers thermally generated. The current is smaller than the theoretical value however, this is due to the effect of a large density of deep trap states in the sample.

In low frequency measurements, the frequency range was from a few hertz to around 30 Khz. The plot of the noise equivalent current, Ieq, at different frequencies is a straight

line with a negative gradient. The result indicated that as frequency was increased from the low frequency range, the corresponding detected noise decreased uniformly. It justified that this noise is inversely proportional to frequency in the low frequency range, i.e. Ieq $\propto \frac{1}{f}$. This is also known as flicker noise. The anthracene sample was thus quite noisy at low frequency.

A plot of DC current verses the noise equivalent current density was made at f = 30 hz. A linear characteristic was exhibited in the log-log plot. The equivalent noise current was found to be proportional to the square of the DC current. This interesting result leads to a speculation that low frequency excess noise in anthracene crystal is a bulk effect rather than a surface states effect.

From the fact that the low frequency power was found to have f^{-1} frequency dependence and is proportional to the square of the DC bias current, it is concluded that the low frequency noise of the device was due to bulk effect which was presumably caused by the distributed trap states. Since a discrete trap state should produce generation-recombination type noise spectrum, the low frequency noise is not due to surface effect. If the surface states are responsible for the low frequency noise, the low frequency noise power should be proportional to I_{DC}^{α} with α much smaller than 2. The energy gap of anthracene is 4.0-4.4 eV. wide. Consequently the deep trap states in anthracene is able to produce large amount of noise

power extended to very low frequencies.

Under high reverse bias condition, microplasma noise was exhibited. The turn-on of a microplasma is a stochastic process. As we assumed that the breakdown phenomenon was a discontinuous two-valued Markoff process having two states, the conducting and the non-conducting, the turn-on of a microplasma would need a triggering carrier. If a triggering carrier does not appear in a microplasma region, the turn-on does not occur even in a sufficient field for ionization and so the turn-on will be ruled by the probability that a triggering carrier appears in a microplasma region. There are many triggering carriers at room temperature which are thermally generated with a constant rate $C_o(T)$. The charge distribution in a trapping centre during the avalanche interval is remarkably deviated from the thermal equilibrium because the thermal generation rate of carriers decreases at low temperature. When avalanche is stopped for a short time, the charge in the trapping centre will be re-emitted to return to the thermal equilibrium distribution. The trapped charges, which are majority carriers, will decrease rather by re-emission than by recombination because the trapped charges can scarcely recombine with minority carriers which seldom exist in the depletion region. As mobile carriers in a depletion layer are swept out immediately, the generation rate of carriers is determined mainly by a trapping center. The thermal equilibrium generation rate can generally be neglected since it is sufficiently small at room temperature

compared with the re-emission rate from the trapping center. The microplasma region is so small that carriers contributing to make the microplasma turn-on are generated only in the very vicinity of the microplasma spot. The relaxation of trapped charges and tunnel emission of them are considered as the re-emission process. As drift velocity is large in a depletion region, retrapping can be neglected. If the change of n_t, the trapped charge density, is governed the thermal relaxation, then

$$\frac{dn_t}{dt} = - n_t \, NS_t V \exp (-E_t/kT) \qquad ...(2)$$

where N is the effective density of state of the band edge to which the trapped charges will be excited, S_t is the trapping coefficient of the trapping coefficient of the trapping center, V is the velocity of carriers, and E_t is the energy difference between the band edge and the trapping center. Accordingly, the generation rate of carriers is given by

$$\frac{d_n}{dt} = n_t \, W + G_o \qquad ...(3)$$

where $W \equiv NS_t V \exp (-E_t/kT)$ and G_o is the thermal carrier generation rate.

Several trapping levels may exist near microplasma region and may contribute to give the observed results. There is a possibility that several microplasma spots turn-on at the same time. If a shallow trapping center exists near the microplasma region, then a local disturbance of the electric field may be caused by such shallow impurities. Such a local disturbance

of impurity distribution has a possibility to cause microplasmas. The theoretical analysis has shown a close agreement to experimental observation of microplasmas.

From the photoconducting test experiment on the sample, it was observed that the output remained the same shape after variation in input bias. However, the pulse magnitude of output was increased slightly corresponding to an increase in bias as well as increase in light intensity. The anthracene photocurrent under room light was found to be approximately two orders of magnitude larger than the dark current. It was also observed that, in the dark, an increase in bias voltage had raised the DC level of output. Under a pulsed light source, there was no increase in DC output level when the input biasing voltage was increased. Under constant room light illumination condition, the output DC level was raised as the bias level was raised. From the above results the author was led to speculate that the anthracene diode would not be a good solid-state light detection device under pulsed or transient type of light source. However under steady state illumination it would be a good light detection device. The behaviour can be explained by the photoresistivity effects of anthracene diode. Since anthracene has a large energy gap, there are many trap states in the crystal. Photoresistivity would be caused by deep trap states. When pulsed light with narrow pulse width and small duty cycle was imparted to the crystal, electrons in deep traps would not have enough time to redistribute themselves and so the output shape

remained the same throughout.

Experiments on temperature dependence of breakdown voltage were performed in order to determine the temperature coefficient. Theoretically the breakdown voltage was predicted to be,

$$V_B(T) = V_B(T_o)\,[1 + \beta(T - T_o)] \qquad \ldots(4)$$

The temperature coefficient, β, was quite accurately measured this way after experimentally determining the breakdown voltage at different temperatures. The method proposed by the author for estimating the breakdown voltage was to use the onset voltage of microplasma. The temperature dependence of onset voltage of microplasma for anthracene crystal was compared with those of the silicon single diodes (Figure 4.2, Figure 4.3 and Figure 4.4). The temperature coefficients in the given temperature range measured this way were constants in these cases. Therefore the onset of microplasma was justified for the representation of breakdown voltage. If the breakdown voltage V_B was otherwise defined, it would be hard to locate V_B experimentally since the junction was soft and as a result the temperature coefficient would not be of constant value. In general, the reverse V-I characteristics of solid-state devices do not exhibit a sharp transition at the breakdown region. There is a gradual bend or knee at the breakdown region and so V_B is not sharply defined as in the ideal case. This is particularly the case for space-charge-limited

anthracene diode. The proposed specification of breakdown voltage in this paper has been supported by experimental evidence which bore close agreement with theory. Therefore it is one of the best methods of estimating breakdown voltage and calculating temperature coefficient.

CHAPTER VII

CONCLUSION

Electrical breakdown in a space-charge-limited anthracene single injection diode is an avalanche breakdown phenomenon. This is justified by the temperature dependence of the postbreakdown current. The postbreakdown current decreases as the temperature is increased and the temperature dependence of the breakdown voltage can be expressed by the following equation

$$V_B(T) = V_B(T_o) \quad 1 + \beta(T - T_o)$$

where β is a positive constant and $V_B(T)$ and $V_B(T_o)$ are the breakdown voltages at temperature T and T_o, respectively. The breakdown voltage can be best estimated by the onset of microplasma noise. Physically, microplasma noise in anthracene solid-state diode is due to a combination of local avalanche breakdown and the local capacitance effect. Microplasma occurs when the diode is biased near the breakdown region and the range in which the diode exhibits microplasma noise depends on the load resistance. It is justified experimentally that the onset of microplasma noise can be applied to measure the temperature coefficient of a solid-state device. This important technical application of microplasma noise has not yet been employed by contemporary researchers. The turn on mechanism of microplasma can be considered as a two-valued Markoff process, consisting of a conducting state and a non-conducting one. The

transition intensity function at room temperature is ruled by the thermal generation rate of carriers. Trap centers near the microplasma have important effects on the turn-on delay of microplasmas which is affected by the re-emission of trapped carriers from the trapping centers near the microplasma region. The theoretical model of microplasma noise agrees well with experimental observations. The temperature coefficient, or the proportionality constant, of anthracene is found to be independent of the charge density in the space charge region.

The low frequency noise of anthracene space-charge-limited diode is a bulk effect. It is a flicker noise characterized by its f^{-1} frequency response and the limiting noise is found to be a thermal noise. The anthracene diode is very noisy at low frequency.

Anthracene diode exhibits large photoresistivity effect. It is a good light detecting device under a steady glow. However, the effect of light detection is largely inhibited when anthracene diode is exposed under a pulsed or transient type of light. The photoeffects on anthracene is still under intense investigation by many researchers.

BIBLIOGRAPHY

1. Armstrong, H.L., "A Theory of Voltage Breakdown of Cylindrical p-n Junctions, with Application," IRE Trans. Electron. Devices, ED-4, 15-16, (Jan. 1957).

2. Armstrong, H.L., "On Avalanche Multiplication in Semiconductor Devices," J. Electron. Control, 5, 97-104, (Aug. 1958).

3. Burgess, R.E., "Statistical Theory of Avalanche Breakdown in Silicon," Can. J. Phys., 37, 730-738, (June 1959).

4. Caywood, J.M., "Photo Emission from Metal Contacts into Anthracene Crystals: A Critical Review," Molecular Crystals and Liquid Crystals, Vol. 12, 1-26, (1970).

5. Champlin, K.S., "Microplasma Fluctuations in Silicon," J. Of Applied Physics, Vol. 30, No. 7, 1039, (July 1959).

6. Chynoweth, A.G. and McKay, K.G., "Internal Field Emission in Silicon p-n Junction," Phys. Rev. 106, 418-426, (1957).

7. Chynoweth, A.G. and Pearson, G.L., "Effect of Dislocations on Breakdown in Silicon p-n Junction," J. Applied Phys. 29, 1103, (1958).

8. Chynoweth, A.G., "Ionization Rates for Electrons and Holes in Silicon," Phys. Review, 109, 537-1540, (March 1, 1958).

9. Chynoweth, A.G. and McKay, K.G., "Photo Emission from Avalanche Breakdown in Silicon," Phys. Rev. 102, 369-376, (April 15, 1956).

10. Chynoweth, A.G. and McKay, K.G., "Threshold Energy for Electron-Hole Pair Production by Electrons in Silicon," Phys. Rev. 108, 29-34, (Oct. 1957).

11. Chynoweth, A.G., "Electrical Breakdown in p-n Junction," Bell Lab. Record, 36, 47-51, (Feb. 1958).

12. Elms, M. and Lowe, A., "Grouping of Microplasma Switching Transients in Silicon Reference Diodes," Solid State Electron. Vol. 14, No. 10, 1055-1056, (1971).

13. Carside, A.E. and Harvey, P., "The Characteristics of Silicon Voltage of Silicon Voltage-Reference Diodes," Proc. Inst. Elec. Engrs. (London), 106, Part B, Suppl 17, 982-990, (May 1959).

14. Cribnikov, E.S., "Avalanche Breakdown in a Diode with a Limited Space-Charge Layer," Fiz. Tverd. Tela, 2, 854-856, (May 1960), (Russian). Translated in Soviet Phys. Solid State, 2, 782-784, (Nov. 1960).

15. Hagenlocher, A.K. and Chen, W.T., "Space-Charge-Limited Current Instabilities in n^{+}-π-$^{+}$ Silicon Diodes," IBM J. Res. Develop., 533-536, (Sept. 1969).

16. Haitz, R.H., Goetzberger, A., Scarlett, R.M. and Shockley, W., "Avalanche Effects in Silicon p-n Junctions, I-Localized Photomultiplication Studies on Micro-plasmas," J. Appl. Phys. 34, 1581-1590, (June 1963).

17. Haitz, R.H., "Model for the Electrical Behaviour of a Microplasma," Bull.-Amer. Phys. Soc. 7, 603, (Dec. 27, 1962).

18. Haitz, R.H., "Variation of Junction Breakdown Voltage by Charge Trapping," Phys. Rev. 138, A260-267, (April 5, 1956).

19. Haitz, R.H., "Mechanisms Contributing to the Noise Pulse Rate of Avalanche Diodes," J. of Applied Phys. Vol. 36, No. 10, 3123, (Oct. 1965).

20. Haitz, R.H., Bull. Amer. Physic. Society II,7, 603, (1962).

21. Haitz, R.H., Bull. Amer. Physic. Society II, 7, 536, (1962).

22. Hsu, S.T., "Avalanche and Associated Light Emission in Molecular Crystals," Appl. Phys. Lett., Vol 20, No. 1, (Jan. 1972).

23. Hsu, S.T., VanDerZiel, A., and Chenette, E.R., "Noise in Space-Charge-Limited Solid-State Devices," Solid-State Electron., 10, 129-135, (1967).

24. Hsu, S.T., "Bistable Noise in p-n Junctions," Solid-State Electron., 14, 487-497, (1971).

25. Hsu, S.T. and Whittier, R.J., "Characterization of Burst Noise in Silicon Devices," Solid-State Electron., 12, 867-878, (1969).

26. Hsu, S.T., "Surface State Related 1/f Noise in p-n Junction," Solid State Electron., 13, 843-855, (1970).

27. Kikuchi, M., "Visible Light Emission and Microplasma Phenomena in Silicon p-n Junction, II-Classification of Weak Spots in Diffused p-n Junctions," J.Phys. Soc. (Japan), 15, 1822-1831, (Oct. 1960).

28. Kikuchi, M. and Tachikawa, K., "Visible Light Emission and Microplasma Phenomena in Silicon p-n Junction," I, J. Phys. Soc. (Japan), 15, 835-848, (May 1960).

29. Maserjian, J., "Determination of Avalanche Breakdown in p-n Junction," J. Of Appl. Phys. 30, 1613-1614, (Oct. 1959).

30. McIntyre, R.J., "Multiplication Noise in Uniform Avalanche Diodes," IEEE Trans. Electron Devices ED-13, 164-168, (Jan. 1966).

31. McIntyre, R.J., "Theory of Microplasma Instability in Silicon," J. of Appl. Phys. Vol. 32, No. 6, 983-995, (June 1961).

32. McIntyre, R.J., "Theory of Microplasma Instability in Silicon," App. Phys., Vol. 32, No. 6, 983, (1961).

33. McKay, K.G., "Avalanche Breakdown in Silicon," Phys. Rev. 94, 877, (1954).

34. McKay, K.G. and McAfee, K.B., "Electron Multiplication in Silicon and Germanium," Phys. Rev. 91, 1079-1084, (Sept. 1953).

35. Miller, S.L.,"Avalanche Breakdown in Germanium," Phys. Rev. 99, 1648, (Sept. 1955).

36. Misawa, T., "Theory of the p-n Junction Device Using Avalanche Multiplication," Prov. IRE, 46, 1954, (Dec. 1958).

37. Moll, J.L., "Physics of Semiconductors," McGraw-Hill,copyright 1964.

38. Newman, R., Dash, W.C., Hall, R.N. and Burch, W.E., "Visible Light from a Silicon p-n Junction," Phys. Rev., 98, 1536-1537, (June 1955).

39. Newman, R., "Visible Light from a Silicon p-n Junction," Phys. Rev., 100, 700-703, (Oct. 1955).

40. Okuto, Y., "Junction Temperature under Breakdown Condition," Japanese J. Of Appl. Phys., Vol. 8, No. 7, 917-922, (1969).

41. Okuto, Y., "The Temperature Coefficient of the Breakdown Voltage of Silicon Abrupt Punched-Through Type Diodes," Japanese J. of Appl. Phys., Vol. 10, No. 1, 154-160, (1971).

42. Rose, F.W., "On the Impact Ionization in the Space Charge Region of p-n Junctions," J.Electron., Contr 1, 3, 396-400, (Oct. 1957).

43. Rose, D.J. and McKay K.G., "Microplasmas in Silicon," Phys. Review, 99, 1648, (Sept. 1955).

44. Rose, D.J., "Microplasma in Silicon," Phys. Review, 105, 413-418, (Jan. 15, 1957).

45. Ruge, I. and Keil, C., Rev. Sc. Instr. 34, 390, (1963).

46. Semitzky, B., and Moll, J.L., "Breakdown in Silicon," Phys. Rev. 110, 612-620, (May 1, 1958).

47. Semitzky, B. and Radin, P.D., "Effect of Internal Heating on the Breakdown Characteristics of Silicon p-n Junctions," J. Appl. Phys. 30, 1945-1950, (Dec 1959).

48. Sherr, S. and King, S., "Avalanche Noise in p-n Junctions", Semiconductor Products, 2, 21-25, (May 1959).

49. Shockley, W., "Transistor Diodes," Proc. Inst. Elec. Engrs. (London), 106, Part 3, Supplement 15, 270-276, (May 1959).

50. Shockley, W., "Problem Related to p-n Junctions in Silicon," Solid-State Electron. 2, 35-67, (Jan. 1966).

51. Shockley, W., Solid-State Electronics 2, 35, (1961).

52. Tauc, J. and Abraham, A., "Thermal Breakdown in Silicon p-n Junctions," Phys. Rev., 108, 936-937, (Nov 15, 1957).

53. Todd, C.D., "Zener and Avalanche Diodes," Wiley Inter-Science, Copyright 1970.

54. Townsend, J.S., "The Passage of Ions in Casses," Nature, 62, 340, (Aug. 1900).

55. VanDerZiel, A., "Solid-State Physical Electronics," Prentice-Hall, Second Edition.

56. Veloric, H.S., Prince, N.D. and Eder, M.J., "Avalanche Breakdown in Silicon Diffused p-n Junction as a Junction of Impurity Gradient," J. Appl. Phys. 27, 895-899, (Aug. 1956).

57. Wolff, P.A., "Theory of Electron Multiplication in Silicon and Germanium," Phys. Rev. 95, 1415-1420, (Sept. 15, 1954).

58. Yamashita, J., "Theory of Electron Multiplication in Silicon," Progr. Theoret. Phys. (Kyoto), 15, 95-110, (Feb. 1956).